

1 Architecture of active extensional faults in carbonates:

2 Campo Felice and Monte D'Ocre Faults, Italian Apennines

3
4 Luca Del Rio^a, Marco Moro^b, Simone Masoch^a, Fawzi Doumaz^b, Michele Saroli^{b,d},
5 Andrea Cavallo^c, Giulio Di Toro^{a,b}

6 ^a Dipartimento di Geoscienze, Università degli Studi di Padova, Via G. Gradenigo 6, 35131 Padua, Italy

7 ^b Istituto Nazionale di Geofisica e Vulcanologia (INGV), Via di Vigna Murata 605, 00143 Rome, Italy

8 ^c Laboratorio tecnologico multidisciplinare CERTEMA, Grosseto, Italy.

9 ^d DICeM-Dip. di Ingegneria Civile e Meccanica, Università di Cassino e del Lazio Meridionale, Via G. Di Biasio 43,
10 03043 Cassino, Italy

11
12 Keywords: Normal faults; Deep-Seated Gravitational Slope Deformations; Carbonates; Damage zones; Slip
13 zones; Apennines.

14
15 Correspondence to: L. Del Rio, Luca.delrio@studenti.unipd.it

16 Telephone number: +39 3317754536

17 ORCID: <https://orcid.org/0000-0002-6648-9641>

19 Abstract

20 To understand better the development of deformation in carbonate-hosted normal faults, we
21 compared the structural architecture of the Campo Felice and Monte D'Ocre active faults in the Italian
22 Central Apennines. The two geometrically linked structures displace the same carbonate sequences,
23 but with different Quaternary slip rates and geological throws. Moreover, several geomorphological
24 features typical of deep-seated landslides were identified across the Mt. D'Ocre range. The Campo
25 Felice fault segment and the southwestern branch of Monte D'Ocre range (the Cama fault segment)
26 consist of 0.4-15 m thick and almost absent fault cores and of > 400 m and < 40 m thick damage
27 zones, respectively. The associated slip zones have different fabrics (i.e., cataclasite vs. crush fault
28 breccia for Campo Felice and Cama Fault, respectively). The different fault zone architecture and

29 associated landscapes would suggest different behaviors of the two faults although similar
30 deformation mechanisms (i.e., cataclasis and pressure-solution) are active in both the two scarps. The
31 Mt. D'Ocre faults would not be segments of the Ovindoli-L'Aquila Fault System and currently
32 accommodate the lateral spreading of the Mt. D'Ocre ridge. Therefore, the seismic hazard associated
33 with the fault system might be reduced. This work shows how macro- to micro-structural (i.e., from
34 km to nm) analyses provide further information to improve the structural characterization of
35 seismogenic sources.

36
37

38 1. Introduction

39 Analysis of natural exposures of fault zones is the best tool to image fault internal structure and
40 to interpret the physical processes associated with fault growth and possibly the ancient seismic
41 activity (Kim et al., 2004; Wibberley et al., 2008; Rowe and Griffith, 2015; Ferraro et al., 2019, 2020;
42 La Bruna et al., 2018; Masoch et al., 2021; 2022). Instead, microstructural analysis of slip zones
43 allows geologists to investigate the deformation mechanisms active during fault zone lifetime (e.g.,
44 Sibson, 1986b; Di Toro and Pennacchioni, 2005; Smith et al., 2011; Tesei et al., 2013; Clemenzi et
45 al., 2015; Leah et al., 2018; Masoch et al., 2019; Ferraro et al., 2019, 2020; Fondriest et al., 2020).

46 The Italian central Apennines are one of the most seismically active regions in Europe, with an
47 average recurrence of one moderate- to large-in-magnitude ($M_w \geq 5.5$) earthquake per decade (Rovida
48 et al., 2020). Most of the Apennines active normal faults strike NW-SE and are often disposed in an
49 *en-échelon* array forming up to 30-km-long fault systems (Boncio et al., 2004; Fig. 1a). Individual
50 fault segments interact with each other and may rupture either independently or together during a
51 seismic sequence. For example, during the Amatrice-Norcia 2016-2017 seismic sequence in the
52 northern Apennines, the M_w 6.5 Norcia October 30, 2016 earthquake, that ruptured the whole Mt.
53 Vettore-Mt. Bove fault system (~ 28-km-long and composed of three fault segments), was preceded
54 by the M_w 6.0 Amatrice August 24, 2016 earthquake in the southern segment and by the M_w 5.9 Visso

55 October 26, 2016 earthquake in the northern segment (Chiaraluce et al., 2017; Villani et al., 2018).
56 Few tens of kilometers to the South, the most recent earthquake that hit the central Apennines was
57 the M_w 6.1 L'Aquila April 6, 2009 earthquake, whereas the largest one instrumentally recorded was
58 the M_w 7.0 Avezzano, 1915 earthquake (EWG, 2010; Fig. 1a).

59 In the area comprised between the Ovindoli and L'Aquila towns, three major fault segments
60 (namely, from north to south: Mt. D'Ocre faults, Campo Felice fault and Ovindoli-Pezza fault; Bosi
61 et al., 1993; Pantosti et al., 1996; Salvi et al., 2003), arranged in a right-stepping *en-échelon* array,
62 form the 27-km-long Ovindoli-L'Aquila Fault System (OAFS; Fig. 1a; also referred as Celano-
63 L'Aquila Fault System in Salvi and Nardi, 1995, and Cerasitto-Campo Felice-Ovindoli-Pezza Fault
64 System in Galli et al., 2008). Thanks to the good correlation among the ages of the Late Pleistocene-
65 Holocene paleo-earthquakes with those recognized along the Ovindoli-Pezza fault (Pantosti et al.,
66 1996), the Mt. D'Ocre faults were interpreted as the northern segment of the OAFS (Salvi et al.,
67 2003). Thus, the Campo Felice and Ovindoli-Pezza faults represent the central and southern segments
68 of the OAFS, respectively (Salvi et al., 2003).

69 In detail, the Campo Felice and Mt. D'Ocre faults displace the same Cretaceous carbonate
70 sequence with similar kinematics, but have (i) different throw rates (1.1 mm/yr vs. 0.2 mm/yr,
71 respectively, estimated in the last 18.000 years; Galadini and Galli, 2000; Salvi et al., 2003) and (ii)
72 border valleys with different shapes and dimensions (i.e., the 20-km²-wide Campo Felice
73 intermontane basin vs. the < 400-m²-wide valleys of the Mt. D'Ocre range; Figs. 1, 2). Moreover,
74 several geomorphological features typical of Deep-seated Gravitational Slope Deformations
75 (DGSDs), such as gravitative trenches, double-crested lines, bulging, up-hill and down-hill facing
76 scarps (Hutchinson, 1988) are recognizable across the Mt. D'Ocre range (Salvi and Nardi, 1995; Salvi
77 et al., 2003; Fig. 1c). In particular, Albano et al. (2015) documented a gravitational subsidence of tens
78 of millimeters of the Mt. D'Ocre ridge toward the L'Aquila Plain in the months following the
79 L'Aquila mainshock (see Fig. 7 in Albano et al., 2015).

80 Specifically, DGSDs are deep gravitational landslides involving hundreds of meters thick rock

81 volumes moving from the ridge-top to the valley floor (Jahn, 1964; Zischinsky, 1966, 1969; Varnes,
82 1978; Hutchinson, 1988; Dramis and Sorriso-Valvo, 1994; Jaboyedoff et al., 2013; Panek and Klimeš,
83 2016; Discenza and Esposito, 2021). DGSDs differs from other types of landslides by both the
84 absence of continuous and well-defined external boundaries (Agliardi et al., 2001, 2012; Crosta et
85 al., 2013) and the lack of a continuous sliding surface or basal shear zone (Dramis and Sorriso-valvo,
86 1994; Discenza and Esposito, 2021), that is commonly buried by the rock-mass and thus almost
87 impossible to recognize, especially in Lateral Spreading DGSDs. The latter usually form when a rigid
88 and joined rock-mass gently overlaps a more ductile and highly deformable bedrock (Varnes, 1978;
89 Hutchinson, 1988; Agliardi et al., 2012; Bozzano et al., 2013; Di Maggio et al., 2014).

90 As a result, the Campo Felice and Mt. D'Ocre extensional faults represent a great opportunity to
91 compare the fault zone associated with two geometrically linked structures displacing the same
92 carbonate rocks, but with different (i) slip rates, (ii) cumulated displacement and (iii) associated
93 morphological features. The internal structure of brittle fault zones commonly includes two main
94 structural units: fault core and damage zone (Caine et al., 1996; Faulkner et al., 2003; Sibson, 2003).
95 The fault core is the high-strain domain usually composed of low-permeability fault rocks (fault
96 gouges, cataclasites and fault breccias) where most of the displacement is accommodated (Ferraro et
97 al., 2018). Instead, the damage zone consists of variably fractured rock volumes where brittle
98 deformation is accommodated by secondary faults and fractures (Chester and Logan, 1986; Agosta
99 and Aydin, 2006; Faulkner et al., 2010; Billi et al., 2003; Choi et al., 2016; Ferraro et al., 2018). In
100 general, the intensity of deformation decreases broadly exponentially from the fault core of the master
101 fault towards the damage zone (Chester and Logan, 1986; Chester et al., 1993; Caine et al., 1996;
102 Faulkner et al., 2003; Wibberley et al., 2008; Mitchell and Faulkner, 2009; Savage and Brodsky,
103 2011; Demurtas et al., 2016; Gomila et al., 2016; Fondriest et al., 2020; Ostermeijer et al., 2020).

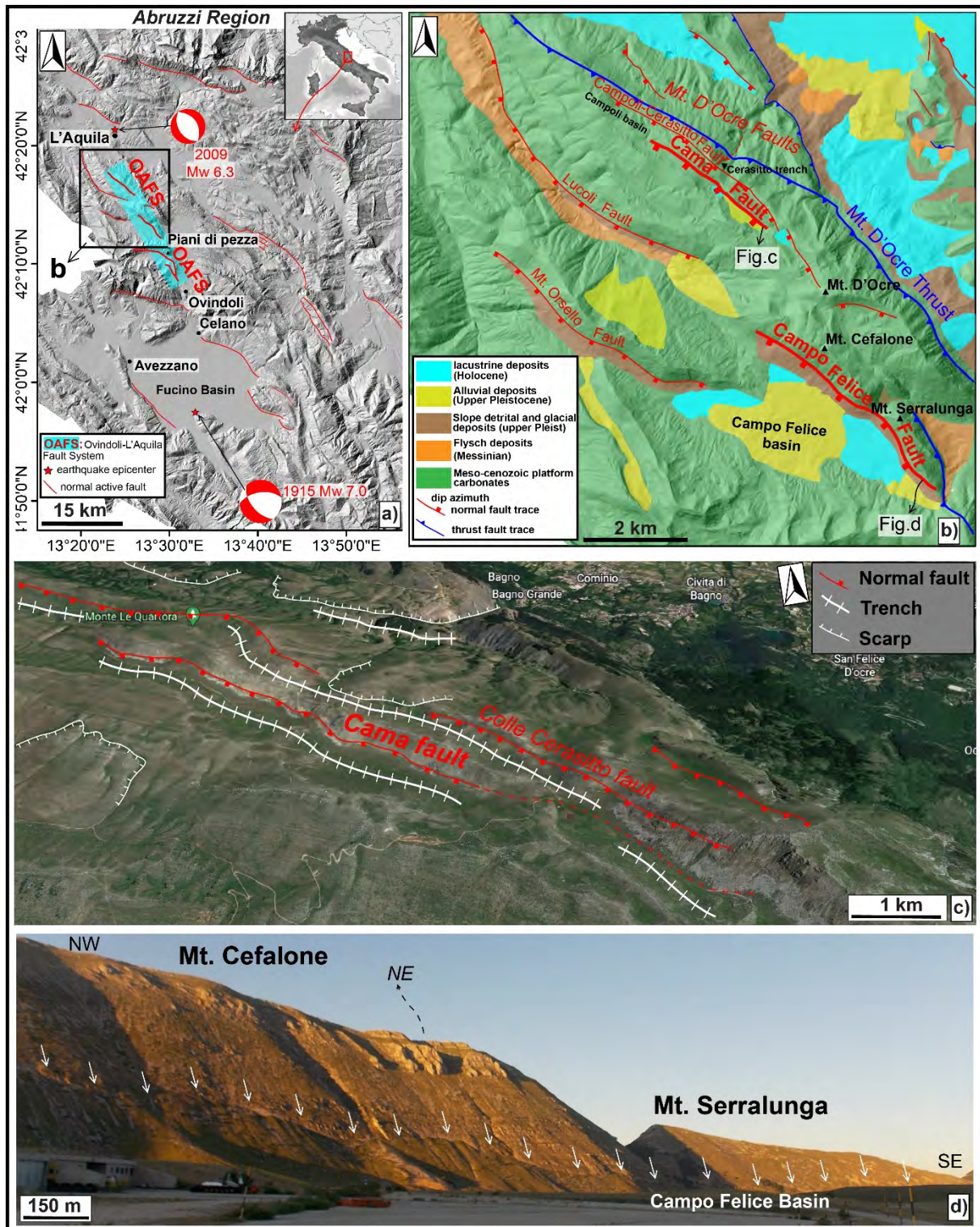
104 In this work, we map and compare the distribution of fractures affecting the footwall blocks of
105 the Campo Felice fault and the southwestern branch of the Mt. D'Ocre faults (i.e., the Cama fault
106 segment; Fig. 1) and analyze the microstructures of the slip zones associated with the major slip

107 surfaces. The analysis of the deformation processes at **macro-** to micro-metric scale (from km to nm)
108 associated with the Campo Felice and Cama fault scarps may contribute to shed more light on 1) the
109 formation and current mechanical behavior of the two faults in the tectonic context of the central
110 Apennines and their relation and, 2) the deformation mechanisms active in the slip zones of
111 carbonate-hosted normal faults as a function of fault displacement. These kind of studies may find
112 more general application to other areas worldwide characterized by moderate to strong seismicity in
113 carbonate rocks. Finally, the possible interpretation of certain sharp scarps as surface expression of
114 seismic or aseismic faulting (i.e., normal faults *vs.* DGSDs; Del Rio et al., 2021) may have strong
115 implications on the characterization of the potential seismogenic source of the area and, thus, to
116 determine the maximum moment magnitude of the earthquake that the fault system can produce
117 (Wells and Coppersmith, 1994; Boncio et al., 2004; Galadini et al., 2012; Falcucci et al., 2016).

118

119

120



121
 122 Figure 1: Geological setting of the Campo Felice and Mt. D'Ocre Faults. a) Seismotectonic map of the study area
 123 (Abruzzi Region) with indicated the main Quaternary active faults (red lines). Thicker red lines indicate the Oivindoli-
 124 L'Aquila Fault System (OAFS). Focal mechanisms indicate the mainshocks of the largest (i.e., Avezzano $M_w = 7.0$,
 125 1915) and most recent (i.e., L'Aquila $M_w = 6.1$, 2009) earthquakes striking the region from 1900. b) Simplified
 126 geological map of the area with the Campo Felice and Cama faults (thicker red lines), investigated in this work. c)
 127 Panoramic view of the Mt. D'Ocre range, with associated geomorphological features typical of DGSDs, such as scarps
 128 and gravitative trenches. d) Surface expression of the Campo Felice fault scarp, affecting the SW slopes of Cefalone
 129 and Serralunga Mts. and bordering the homonym intermontane basin.

130 2. Geological setting

131 2.1. Tectonics of the Apennines

132 The Italian Apennine fold-and-thrust belt started to develop since Miocene, due to the NE-
133 verging collision between the Adriatic and European Plates (Elter et al., 1975; Patacca et al., 1992a;
134 Carminati et al., 2012). The Apennine orogenesis was characterized by a general eastward migration
135 of the chain thrust front and consequent formation of piggy-back basins associated with the main
136 thrusts (Cosentino et al., 2010). In the central Apennines, during this compressional phase, shallow-
137 water and pelagic Mesozoic-Cenozoic limestones were juxtaposed to syn-orogenic foredeep deposits
138 by NE-verging thrusts (Cosentino et al., 2010). Since Upper Messinian to present, a NE oriented
139 crustal extension accommodated the stretching of the Apennine chain, caused by the retreat of the
140 subduction hinge toward E-NE (Malinverno and Ryan, 1986; Carminati and Doglioni, 2012). During
141 Quaternary, a strong increase in regional uplift (i.e., more than 1000 m; D'Agostino et al., 2001) lead
142 to the formation of large intermontane basins filled with continental deposits, bordered by active
143 normal faults (Demangeot, 1965; Dramis, 1992; Galadini and Galli, 2003). The combination of
144 extensional faulting (Quaternary extension rate of 2-3 mm/yr; Hunstad et al., 2003) and regional uplift
145 is the main cause of the development of DGSDs in the central Apennines (Galadini, 2006).

146 The current extensional tectonic phase is accommodated by active normal faults cutting and
147 locally exploiting the inherited Miocene-Early Pleistocene thrusts and the earlier Mesozoic normal
148 faults (Elter et al., 1975; Vezzani et al., 2010; Leah et al., 2018; Lucca et al., 2019; Fondriest et al.,
149 2020). Most of the active faults in central Apennines strike NW-SE (i.e., “Apennine trend”) and are
150 commonly organized in fault systems with associated intermontane basins (e.g., Campo Felice and
151 Middle Aterno Basins; Bosi et al., 1993; Cavinato et al., 2002). Smaller NE-SW oriented normal
152 faults (i.e., “anti-Apennine trend”) are also spread in the area.

153

154 2.2. Campo Felice and Mt. D'Ocre Faults

155 In the area affected by the Campo Felice and Mt. D'Ocre Faults, Cretaceous and Miocene
156 shallow-water carbonates belonging to the Latio-Abruzzi succession crop out. The carbonate
157 sequence is locally capped by Upper Miocene hemipelagic marls and Messinian flysch deposits
158 (Cosentino et al., 2010; Brandano, 2017; Figs. 1b; 2a, b). The Cretaceous Units record the
159 sedimentation in shallow-water platform environments along the passive margin of the Adriatic plate,
160 started during Middle Liassic. These units mainly consist of micritic limestones alternated with thin
161 levels of calcarenites or marls, with bedding thickness ranging from tens of centimetres to over one
162 meter (see stratigraphic column in Fig. 2a). During the Lower Albian-Early Cenomanian, this
163 carbonate platform underwent three periods of aerial exposure and erosion of the underlying
164 limestones, with consequent formation of karst cavities filled with bauxitic deposits (i.e., IBX fm. in
165 Fig. 2; Mancinelli et al., 2003). Middle Miocene carbonates (i.e., "*Calcari a Briozoi e Litotamni*")
166 Formation) consist of thin whitish calcarenites including bryozoans, lithotamnia and corals (Fig. 2a)
167 that deposited unconformably or para-conformably above the Cretaceous limestones (i.e., "Paleogene
168 Hiatus"; Damiani et al., 1992). Miocene hemipelagic marls record the gradual drowning of the
169 carbonate ramp with consequent increase in clay amount at the expense of lime portion. During
170 Messinian, siliciclastic turbidites filled the foredeep basins according to the eastern migration of the
171 Apennine chain thrust front (Patacca and Scandone, 1989; Figs. 1b, 2a).

172 The Campo Felice Fault strikes NW-SE for ~ 6 km, cutting the south-western flanks of Mt.
173 Serralunga, to SE, and Mt. Cefalone, to NW (Figs. 1b, d; 2a). The fault has a normal dip-slip
174 kinematics (Wilkinson et al., 2015) and juxtaposes Cretaceous shallow-water limestones with talus
175 and slope sediments deposited during and after the Last Glacial Maximum (i.e., ~ 25.000-21.000
176 B.P.; Dramis, 1983). The Campo Felice fault borders to SW the homonym intermontane basin (~ 20
177 km² wide), filled with Late Pleistocene to Holocene alluvial, lacustrine and glacial deposits (Giraudi
178 et al., 2011; Figs. 1b, 2a). The Mt. D'Ocre thrust borders the north-eastern side of Serralunga and
179 Cefalone Mts. juxtaposing pre-orogenic calcareous units with syn-orogenic calcareous and
180 siliciclastic deposits (Figs. 1b, 2a, c).

181 The Mt. D'Ocre range is composed of three parallel and discontinuously outcropping bedrock
182 scarps, from the Mt. D'Ocre, to SE, to the Campoli Basin, to NW, affecting the same rocks of the
183 Campo Felice fault (Salvi et al., 2003; Figs. 1b, d; 2b). The largest scarp belongs to the Campoli-
184 Cerasitto fault (~ 9.5 km long along-strike), that borders to SW the Campoli Basin in the northwestern
185 sector (Salvi et al., 2003; Fig. 1b). Instead, the Cama fault is ~ 3-km-long and borders three small and
186 narrow valleys (i.e., Cama, Vallefredda and Santo Lago valleys to SW), possibly produced by the
187 gravitational spreading of the ridge-top (Salvi et al., 2003; Fig. 2b).

188

189

190 3. Methods

191 We realized two geological maps of the area affected by the Campo Felice and the Mt. D'Ocre
192 faults (Fig. 2a, b) by editing and drawing the geological and stratigraphic information reported in the
193 1:50.000 scale geological map from ISPRA ("Foglio 359 L'Aquila") over a shaded relief from
194 TINITALY (Triangular Irregular Network of Italy) 10-m-resolution digital elevation model (Tarquini
195 et al., 2007). From the geological maps, we built two cross-sections oriented perpendicular to the
196 strike of the Campo Felice and Mt. D'Ocre faults, respectively, to estimate the geological throw (i.e.,
197 the vertical component of displacement) and identify possible differences at regional scale associated
198 with the two structures. The geological throw was calculated as the elevation difference between the
199 hanging wall and footwall cutoffs of a selected Cretaceous unit (Fig. 2c, d). We assumed a constant
200 thickness of the geological units across the two sections.

201 High-resolution georeferenced orthomosaics (spatial resolution of ~ 3 cm/pixel) of Cefalone and
202 Serralunga Mts. and the ridge crest affected by the Cama fault were produced by stitching hundreds
203 of either nadir-directed and fault plan-parallel photographs taken with a MAVIC 2 Pro drone and
204 processed with Agisoft Metashape Pro software. The Stitching or Mosaicking process has been made
205 possible thanks to photogrammetric processing, producing hence, a high-resolution DEM and 3D

206 mesh used as base to ortho-rectify the final mosaic of the drone pictures. Original field structural
207 surveys were conducted to map the footwall block of the Campo Felice and Cama faults. We defined
208 five main structural units based on field observations, such as: 1) average spacing among fractures 2)
209 clast/matrix proportion in the fault rocks and 3) degree of preservation of primary sedimentary
210 structures (Fig. 3). The trace of master fault scarps and of larger secondary faults (i.e., faults with
211 lateral continuity > 2 m and with a fault core associated), and the spatial distribution of the different
212 structural units were reported in topographic maps at 1:1000 scale (spatial resolution of 0.2 m/pixel)
213 provided by the Abruzzi Geoportal (www.geoportale.regione.abruzzo.it). These data were digitalized
214 with ArcGIS 10.7.1 software, using the produced orthomosaics as base map, to realize detailed
215 structural maps of the footwall blocks of the Campo Felice and Cama fault zones. The distribution of
216 the structural units was drawn with higher degree of transparency where they were not directly
217 observed, but inferred during the field surveys. Three structural-geological cross-sections across the
218 analyzed fault zones were produced (Figs. 4-6).

219 Structural data (n = 3047) were collected along the whole along-strike path of the outcropping
220 master fault scarps and across the footwall damage zones and located with a handheld GPS (accuracy
221 ± 2 m). We systematically measured the attitude of different structural and stratigraphic elements
222 (i.e., bedding, fractures, major and secondary faults, veins, stylolites). Where possible, the kinematic
223 of the secondary faults was measured through kinematic indicators, such as S-C fabrics, grooves,
224 slickenlines and/or calcite slickenfibers (Chester and Logan, 1987; Petit, 1987). Structural
225 measurements were plotted and analyzed using stereonet (lower hemisphere, Schmidt equal area)
226 created with OSX Stereonet software (Allmendinger et al., 2011; Cardozo and Allmendinger, 2013).

227 From 30 samples collected from the major and secondary faults, we selected 14 samples to
228 produce syton-polished thin sections cut perpendicular to the slip surface and parallel to the kinematic
229 indicators (where recognizable, otherwise along the fault dip direction). The thin sections were photo-
230 scanned at high resolution (4000 dots per inch) both in plane and cross polarized Nicols and edited

231 using specific tools of Adobe Photoshop to highlight the clast shapes, minor fractures and veins and
232 the texture of the fine matrix surrounding the clasts.

233 Transmitted-light optical microscopy (OM) was used to determine microstructural features at
234 thin section scale and to identify areas suitable for microanalytical investigations. Scanning electron
235 microscopy (SEM) was used to acquire high-resolution backscattered electron (BSE) images coupled
236 with both semiquantitative and quantitative energy dispersion spectroscopy (EDS) elemental
237 analysis. SEM investigation were performed with a CamScan MX3000 (max. resolution ~ 50 μm in
238 back-scatter electrons) installed at Dipartimento di Geoscienze (Università degli Studi di Padova,
239 Padova, Italy) and with the field-emission SEM (FESEM) Merlin Zeiss (resolution of 10-100 nm in
240 Back-Scatter electrons, BSe, and of 300 nm to 1 μm in X-rays) installed at CERTEMA laboratory
241 (Grosseto, Italy). The images were taken with an acceleration voltage of 15 kV and a working distance
242 of 8.5-5.3 mm.

243

244

245 4. Results

246 In this section, we describe two geological sections cross-cutting the Campo Felice and Cama
247 fault zones, the fault architecture in the footwall blocks and the microstructures observed in the slip
248 zones associated with the major and secondary fault surfaces. Faults traced with dashed lines in the
249 cross-sections indicate both the faults inferred in map and the interpreted prosecution of the major
250 faults at depth. In the case of two normal faults with opposite dip direction and crossing each other at
251 depth, we interpret the normal fault with higher displacement as cutting the one with lower
252 displacement.

253

254

255 4.1 Geological cross-sections

256 The cross-section A-A' (~ 8-km-long) is oriented SW-NE from Mt. Puzzillo to Mt. Cagno and
257 crosses the Campo Felice basin, the Campo Felice fault, the central sector of Mt. Cefalone and the
258 Mt. D'Ocre thrust (Fig. 2a, c). Unfortunately, though active seismic investigations were conducted
259 by the Istituto Nazionale di Geofisica e Vulcanologia in 2019-2021, no geological and geophysical
260 data are currently available to infer the Cretaceous-Miocene stratigraphy and possible secondary
261 structures in the Campo Felice basin. Therefore, assuming a constant dip of ~ 30° of the geological
262 Units, we estimate a maximum geological throw of ~ 1050 m associated with the Campo Felice fault
263 in this sector (with a possible overestimate of ~ 400 m in case of sub-horizontal dip) from the elevation
264 difference between hanging wall and footwall cutoffs of the Cenomanian Intrabauxitic limestones
265 (IBX fm.; Fig. 2c). Because of the large displacement associated, we assumed that the Campo Felice
266 fault cuts the Mt. D'Ocre thrust at depth. Instead, we interpret the other normal faults at the hanging
267 wall of the Campo Felice fault to flatten at depth along the Mt. D'Ocre thrust because of their lower
268 displacement. Here, the latter puts in contacts Lower Cretaceous shallow-water carbonates with
269 Upper Miocene syn-orogenic limestones forming a large ramp anticline cut by small faults with tens
270 of meters of displacement (Fig. 2c).

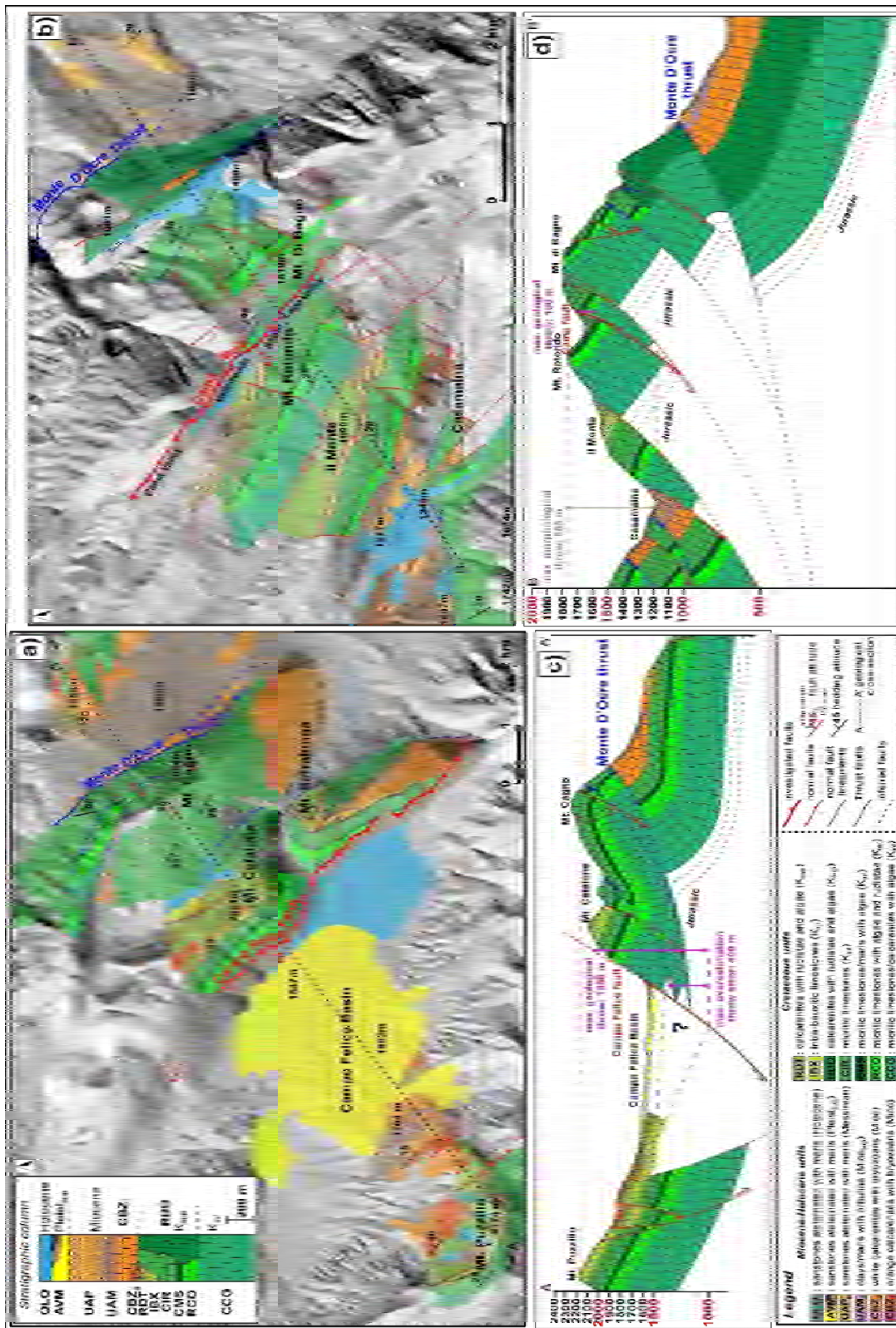
271 The cross-section B-B' (~ 7.25-km-long) cross-cuts the entire Mt. D'Ocre range, located at the
272 hanging wall of Mt. D'Ocre thrust. In our geological map (Fig. 2b), we trace the Cama fault up to the
273 south-eastern termination of the Santo Lago Valley for two reasons: (1) the stratigraphic relations
274 among Cretaceous carbonates infer the presence of a SW-dipping normal fault with a geological
275 throw of ~ 100 m (Fig. 2d); (2) the presence of a sharp fault scarp cropping out discontinuously along
276 the western slope of Vallefredda and Santo Lago Valleys (Figs. 1c, 5). Because of the relatively low
277 associated displacement, the Cama fault was interpreted to flatten on the Mt. D'Ocre thrust at depth,
278 as well as the other normal faults of the Mt. D'Ocre Range (Fig. 2d). The latter juxtaposes shallow
279 water Cretaceous carbonates with Messinian turbiditic deposits (Fig. 2b, d). According to our
280 interpretation, the Mt. D'Ocre thrust does not flatten on turbidites, but forms a ramp to accommodate
281 the folding of both Cretaceous and Miocene Units (Marshak et al., 2019). The maximum

282 morphological throw associated with the faults bordering the western side of Il Monte and Rotondo
283 Mts. is ~ 600 m, calculated from the elevation difference between the top of Mt. Rotondo and the
284 lower portion of the basin hosting the Casamaina Village (Fig. 2d).

285

286

287



288 Figure 2: Simplified geological maps of the areas affected by the Campo Felice (a) and Mt. D’Ocre (b) faults, including
 289 stratigraphic column and trace of the cross-sections. Data are compiled from the 1:50.000 scale “Foglio 359 L’Aquila”
 290 (ISPRA). c) Cross-section A-A’, showing the Campo Felice fault cutting Cretaceous platform carbonates with a
 291 maximum estimated geological throw of ~1050 m (with a possible overestimate of ~400 m). d) Cross-section B-B’,
 292 cutting the entire Mt. D’Ocre range, at the hanging wall of the Mt. D’Ocre thrust. The Cama fault displaces Cretaceous
 293 carbonates with ~100 m of geological throw.

294 4.2 Fault zones architecture

295 In this section, we describe the spatial distribution and attitude of secondary faults and fractures
296 in the footwall of the Campo Felice and Cama fault zones (~ 6 km and ~ 3 km long, respectively; Fig.
297 1). Though the two faults cut the same host rocks (Figs. 1, 2), their fault architecture (i.e., core and
298 damage zone thickness and distribution, type and intensity of fault/fracture network) may suggest
299 different formation mechanism, evolution and deformation styles. We use the terms open fractures or
300 fissures to indicate fractures with > 1 cm of aperture between the two opposite fracture surfaces,
301 locally filled by unconsolidated soil deposits (e.g., Figs. 3a, 7h; Fossen, 2010). Instead, extensional
302 (or Mode-1) fractures refer to regularly spaced fractures with similar attitude, forming specific sets,
303 with no displacement between the fracture surfaces (Engelder, 1987; Pollard and Aydin, 1988;
304 Fossen, 2010). The five main structural units identified in the field are described from the lower to
305 higher strained ones as follows:

306 **Host rocks with fissures** (brown in the structural maps; e.g., Figs. 3, 6) consist of rock volumes
307 where intact carbonate strata are affected by sub-vertical (> 60°) fractures and fissures spaced > 20
308 cm apart, with fracture surfaces very rough due to karst-related processes (Fig. 3a).

309 **Weakly fractured rocks** (light blue in the structural maps; e.g., Figs. 3-6) consist of poorly
310 fractured rock volumes, where bedding is clearly recognizable and not affected by fractures, which
311 are usually spaced > 10 cm apart and oriented at high angles (i.e., 60°-90°) with respect to the bedding
312 surfaces, as a result forming lozenge-like structures (Fig. 3b).

313 **Fractured rocks** (yellow in the structural maps; e.g., Figs. 3-6) consist of fractured rock
314 volumes, where bedding surfaces are still clearly recognizable and rarely cut by fractures. The latter
315 are both sub-vertical (i.e., dip angle > 65°) and sub-horizontal (i.e., dip angle < 20°) with respect to
316 the bedding surfaces and spaced 3-10 cm apart (Fig. 3c).

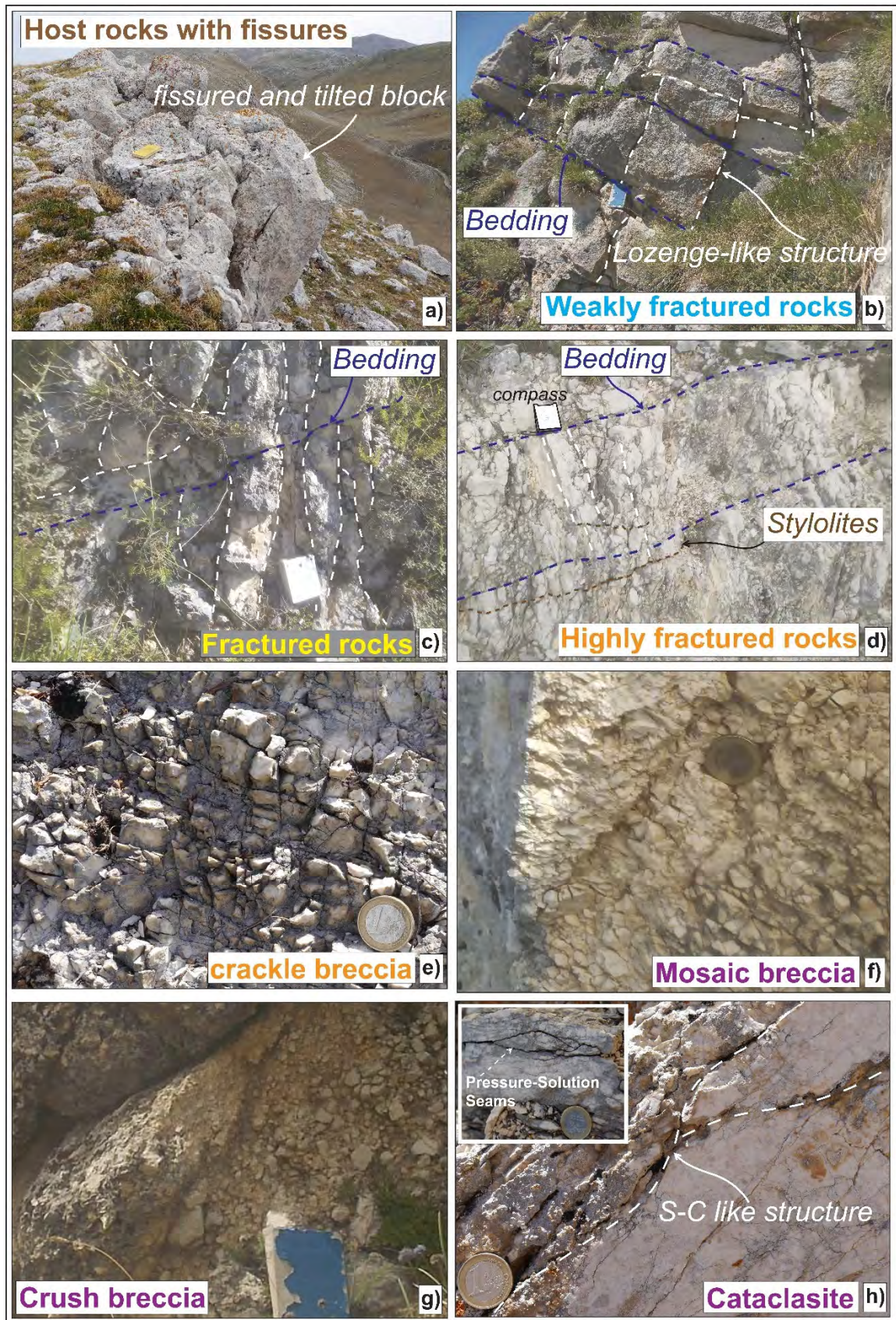
317 **Highly fractured rocks** (orange in the structural maps; e.g., Figs. 3-6) consist of highly fractured
318 rock volumes, with strata partially recognizable (Fig. 3d). Extensional fractures are oriented both sub-
319 vertical and at 40°-55° with the bedding surfaces, with 1-3 cm of spacing among fractures, or sub-

320 horizontal, spaced 1-15 cm apart. Where fracture abundance increases (i.e., where both sub-vertical
321 and sub-horizontal fractures are spaced ~ 1 cm apart), the highly fractured rocks appear as crackle
322 breccias (i.e., incohesive fault breccia with > 75% of clasts > 2 mm; Woodcock and Mort, 2008; Fig.
323 3e). Highly fractured, Fractured and Weakly fractured rocks represent the footwall damage zone of
324 the studied fault zones. Highly fractured and Fractured rock volumes usually crop out close to or few
325 meters away from the master fault surface or in areas strongly affected by secondary faults.

326 **Cataclasite/Breccias** (purple in the structural maps; e.g., Figs. 3-6) consist of crush breccias and
327 incohesive mosaic breccias composed of angular host-rock-built fragments (~ 5 mm to 10 cm and ~
328 5 mm to 2 cm in size, respectively) surrounded by a fine matrix (~ 10% of total volume; sensu
329 Woodcock and Mort, 2008; Fig. 3f, g) and cohesive fault rocks with ultra-cataclastic (i.e., > 90% of
330 fine calcite matrix), cataclastic (i.e., 90-50% of fine matrix; Fig. 3h) or proto-cataclastic fabrics (i.e.,
331 50-10% of fine matrix). In these volumes, bedding surfaces and other sedimentary structures (e.g.,
332 stromatolitic laminations or “burial” stylolites/pressure-solution seams) are not recognized.

333

334



335

336

337

338

339

Figure 3: Main structural units identified across the Campo Felice and Cama fault zones. a) Host rock with fissures, very large and locally causing the tilt of carbonate blocks down to the valley. b) Weakly fractured rocks, with high angle fractures (dotted white lines) forming lozenge-like structures. c) Fractured rocks affected by sub-vertical fractures spaced 3-10 cm apart. d) Highly fractured rocks, with subvertical fractures usually cut by stylolites striking sub-parallel

340 with the bedding surfaces. e) crackle breccias, where fractures are spaced ~ 1 cm apart. f-h) Mosaic breccias, crush
341 breccias and cataclasites, with pressure-solution seams and S-C like structures caused by pressure-solution processes.
342 WGS84 GPS Location: 42.286720°N, 13.393950°E (a); 42.235224°N, 13.437680°E (b); 42.219666°N, 13.460662°E
343 (c); 42.226981°N, 13.453245°E (d); 42.223688°N, 13.455338°E (e); 42.220531°N, 13.459215°E (f); 42.233561°N,
344 13.438081°E (g); 42.238451°N, 13.431004°E (h).

345
346
347

348 4.2.1 The Campo Felice fault

349 The Campo Felice master fault is exposed along the western slope of Cefalone and Serralunga
350 Mts. with a ~ 5.8-km-long fault scarp (Figs. 4, 5). The fault scarp has an average height of about 3-4
351 m (up to 15 m in some sectors; Fig. 7a) and crops out almost continuously along Cefalone Mt.,
352 whereas it is less continuous and more wavy along-strike along Serralunga Mt. (Figs. 4, 5). The
353 exposed fault surface is very sharp, but also strongly karstified, except in the south-eastern tip. Here,
354 in the areas where the fault cuts the bauxitic levels, the fault surface is locally well preserved and
355 appears very polished (Fig. 7b). The fault dips 45°-75° (mean dip angle of 55°) to SW and sharply
356 truncates the carbonate host rocks, dipping 5°-50° to NW (see stereonet in Figs. 4-5). In contrast,
357 along the numerous left-stepping transfer zones, the master fault surface dips to SSW-SE and the host
358 rocks dip towards SW in the relay ramp (see bedding and master fault stereonet in Figs. 4, 5).

359 Fracture abundance increases close to the master fault and within the step-over zones, where the
360 fault core and Highly fractured rocks crop out. The fault core units mainly consist of (i) cataclasites
361 with white to reddish matrix (< 40-cm-thick, up to 3-m-thick in the step-over zones; Figs. 3h, 7c) and
362 (ii) fault breccias (Fig. 3g, 4b), commonly 50-cm- to 2-m-thick, up to 5-15-m-thick in the master fault
363 step-overs and bends (see cross-section A-A' in Fig. 4). Highly fractured volumes crop out close to
364 either the master fault or the fault core with a thickness of 15-150 m. Both Highly fractured and
365 cataclastic rocks are cut by calcite-bearing veins and by numerous steeply dipping (60° to 90°)
366 secondary faults (Figs. 5b, 7d) that mainly strike NW-SE and dip both synthetically (i.e., with similar
367 dip azimuth) and antithetically (i.e., with opposite dip azimuth) with respect to the master fault (see

368 stereonet in Figs. 4, 5). In the fault core, minor secondary fault surfaces also strike N and E. Where
369 the fault surfaces are very polished, the kinematic indicators show a normal dip-slip and rarely strike-
370 slip kinematics (Figs. 5, 7c). In the central sector, extensional fractures are arranged in several sets
371 striking from SSE to NE and from N to S, consistent with the orientation of the secondary faults (Figs.
372 4, 5). Most of the fractures are oriented at high angle (i.e., 60-90°) with respect to the bedding surface
373 and are usually cut by fractures with 40°-55° of dip angles (Figs. 3d, 4c).

374 Fracture abundance within the damage zone slightly decreases towards the master fault tips (i.e.,
375 average fracture spacing > 3 cm), particularly in the north-western sector, where Fractured rock
376 volumes (Fig. 3c) are more abundant, but still affected by numerous secondary faults (Figs. 4, 5).
377 Here, the fractures mainly dip from SE to NW both at high (i.e., > 65°) and low angles (i.e., < 35°)
378 without cutting the bedding surfaces (Figs. 3c, 4-5). High angle fractures are spaced 3-10 cm apart
379 and usually cut the low angle ones, spaced up to 1 m apart (Fig. 4d). Fracture intensity drastically
380 decreases ~ 60-120 m away from the master fault surface, where the host rocks are cut by sub-vertical
381 fractures spaced > 10 cm apart and are not affected by secondary faults (Fig. 3b, 4e). Fractured rocks
382 usually represent the transition unit between Highly (Fig. 3d) and Weakly fractured domains (Fig.
383 3b), although sharp contacts between these two units were also observed, due to the presence of a
384 large secondary fault or an abrupt change in the thickness of the carbonate strata (i.e., from ~ 1 m to
385 20-30 cm).

386 The fault core (~ 15-m-thick) and damage zone units extend for > 400 m across a large incision
387 feeding the fan located in the middle sector of Mt. Cefalone (see cross-section A-A' in Fig. 4). In this
388 area, the abundance of fractures affecting the host rocks gradually decreases (i.e., from < 1 cm to >
389 10 cm of fracture spacing) up to ~ 150 m away from the master fault. Then, Fractured rocks (Fig. 3c,
390 4d) crop out across the incision for ~ 160 m, after which less fractured volumes are exposed. In the
391 latter, the fractures are spaced 15-30 cm apart and dip sub-vertically (dip angles of 65°- 90°) towards
392 SW and NE cutting > 1-m-thick carbonate strata (Fig. 4e). In both fault core and damage zone,
393 pressure-solution processes result in the formation of seams and stylolites striking parallel to the

394 bedding strata, usually cutting calcite veins and subvertical fractures and locally displaced by
395 fractures oriented at 40° - 55° with the bedding surfaces (Figs. 3d, 4c, d). Furthermore, in both the fault
396 core and Highly fractured domains, pressure-solution also allow the development of S-C like
397 structures at different scales (e.g., Figs. 3h, 4c, 7e).

398

399

400 4.2.2 The Cama fault

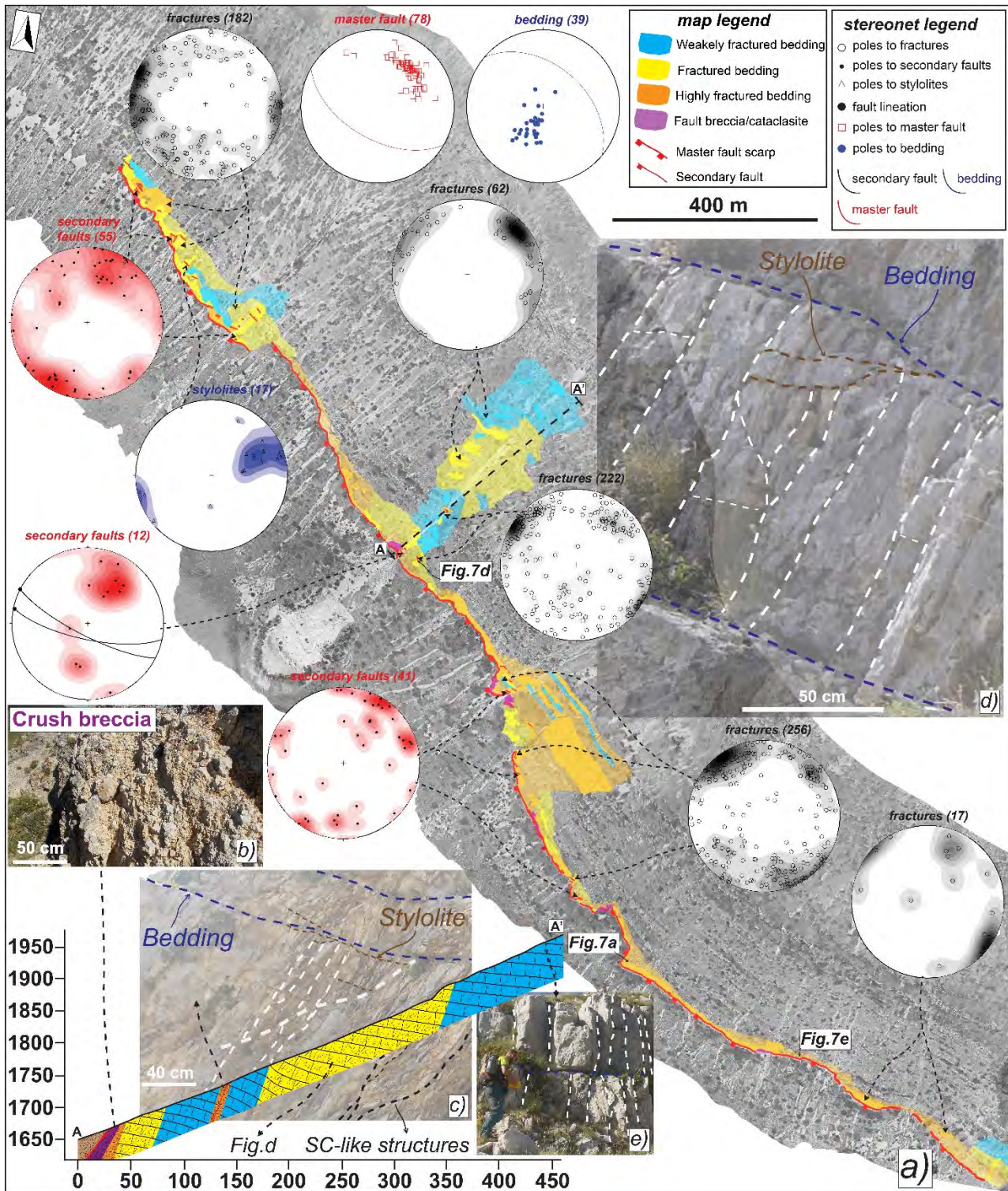
401 The Mt. D'Ocre range is composed of three NW-SE oriented fault branches spreading from Mt.
402 D'Ocre, to SE, to the Campoli Basin, to NW (Fig. 1b). The Cama fault represents the south-western
403 branch of the Mt. D'Ocre range. Our fieldwork surveys were conducted along this fault because of
404 the very sporadic outcrops of the major scarp and footwall host rocks associated with the larger
405 Campoli-Cerasitto fault (Fig. 1b). The Cama fault is ~ 3.4-km-long and borders the Cama Valley in
406 the north-western sector and Vallefredda and Santo Lago Valleys in the middle and south-eastern
407 sectors, respectively (Figs. 1c, 2b, 6). The fault scarp crops out mainly in the middle and southern
408 sectors (maximum height of ~ 2 m), although discontinuously (Fig. 6). The scarp dips 49° - 70° (~ 60°
409 on average) to SW and affect the same carbonate rocks in the footwall of the Campo Felice fault. The
410 host rocks dip to N-NE with 20° - 45° of dip angles up to 100 m away from the master fault scarp (Fig.
411 7f) and with 50° - 70° of dip angles close to the hill crest (Fig. 6c).

412 Both the fault core and the damage zone crop out for a total thickness < 40 m. The fault core
413 crops out only close to the south-eastern tip, where it is ~ 1-m-thick and mainly consist of crush
414 breccias, whereas Highly fractured (Fig. 6b) and Fractured rocks (up to 15-30 m in thickness) are
415 mainly distributed in the area located between Vallefredda and Santo Lago Valleys. In these domains,
416 none secondary fault was observed and only few calcite veins (< 4 mm thick) associated with the
417 major scarp, mostly arranged in conjugate systems, were mapped (Figs. 6, 7g). Mode I fractures are
418 mainly oriented at high angles with respect to the bedding surfaces and largely scattered in dip
419 attitude, forming different sets usually conjugated themselves (Fig. 6). As in the case of Campo Felice

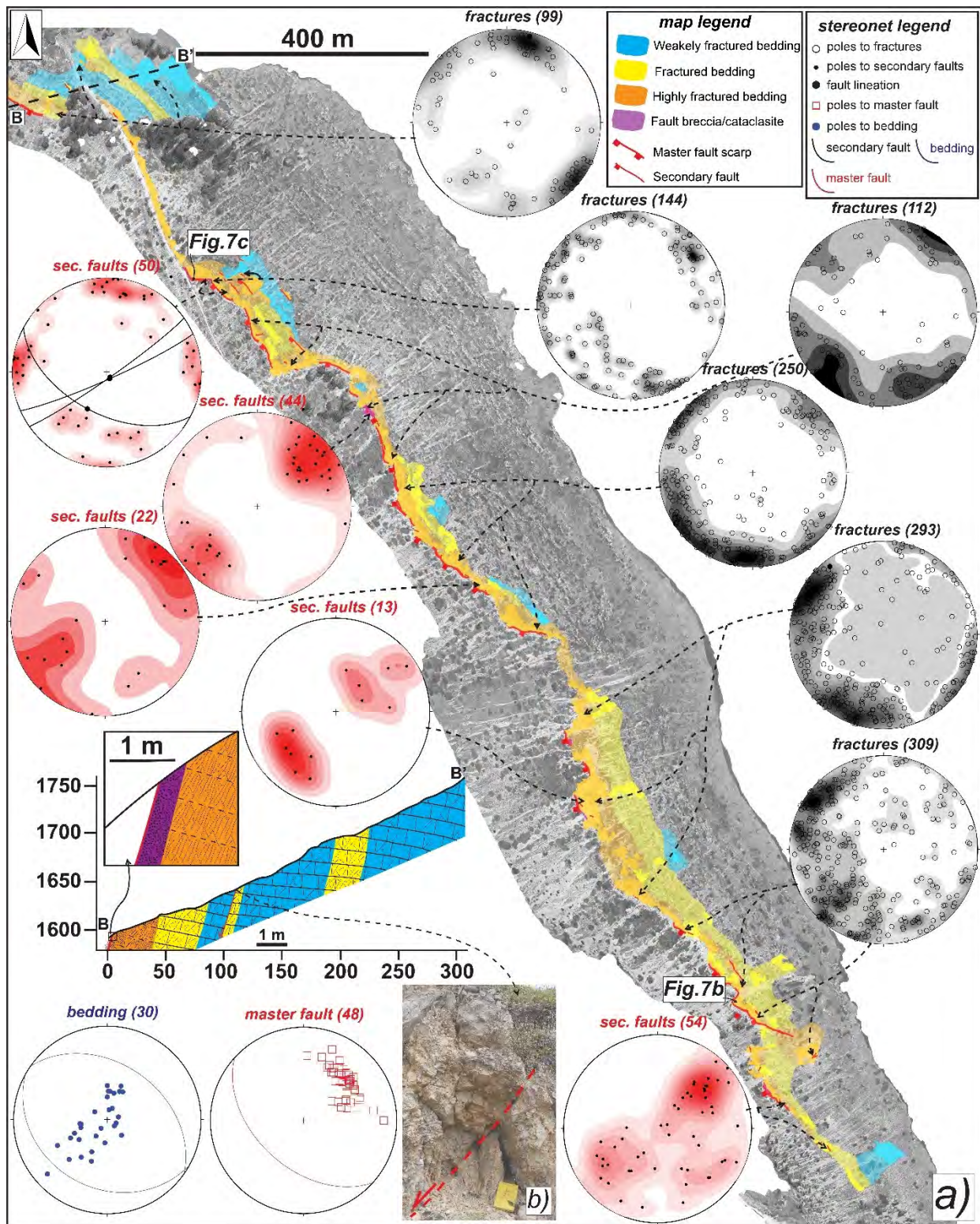
420 fault, in the few areas close to the master fault in which the spacing among fractures is less < 3 cm,
421 pressure-solution processes contribute to the formation of S-C like structures (Fig. 6b).

422 Where the damage intensity decreases along the master fault, 15-to-35-m-thick Weakly fractured
423 domains (Fig. 3b) crop out, with both sub-vertical (i.e., dip angles of 60°-90°) fractures and fissures
424 (< 2 cm of aperture) spaced > 10 cm apart. Outside the damage zone, starting from ~ 40 m to the NE
425 from the master fault surface till the hillcrest top, the host rocks are almost undeformed and only
426 affected by high angle sub-vertical fractures and fissures (1-20 cm of aperture) spaced 20 cm to 1 m
427 apart and with scattered dip attitude (i.e., Host rocks with fissures domain; Fig. 3a, 6). In this sector,
428 the bedding and fracture/fissure surfaces are very rough, possibly due to karst processes (Figs. 3a, 6).
429 Moreover, moving up to the hillcrest top, most fissured blocks are tilted by gravity towards the valley
430 slope (Figs. 3a, 7h).

431



432
 433 Figure 4: a) Structural map of the Campo Felice fault zone in the Mt. Cefalone sector, cross-section (NE oriented)
 434 across the fault zone and structural data collected within the different structural units, plotted in Equal Area-Lower
 435 Hemisphere stereonet with density contours areas (see figure legend for symbols description). The inferred distribution
 436 of the structural units was drawn with higher degree of transparency. b) Fault core consisting of crush breccias. c)
 437 Highly fractured rocks, affected by high angle fractures (dotted white lines) spaced < 3 cm apart, cut by lower angle
 438 fractures and bedding parallel stylolites, and locally forming S-C like structures. d) Fractured rocks, consisting of > 1-
 439 m-thick carbonate strata affected by high angle fractures spaced < 10 cm apart, cut by stylolites. e) Weakly fractured
 440 rocks, cut by high angle fractures spaced > 10 cm apart.



441

442 Figure 5: a) Structural map of the Campo Felice fault zone in the Mt. Serralunga sector, cross section (ENE oriented)

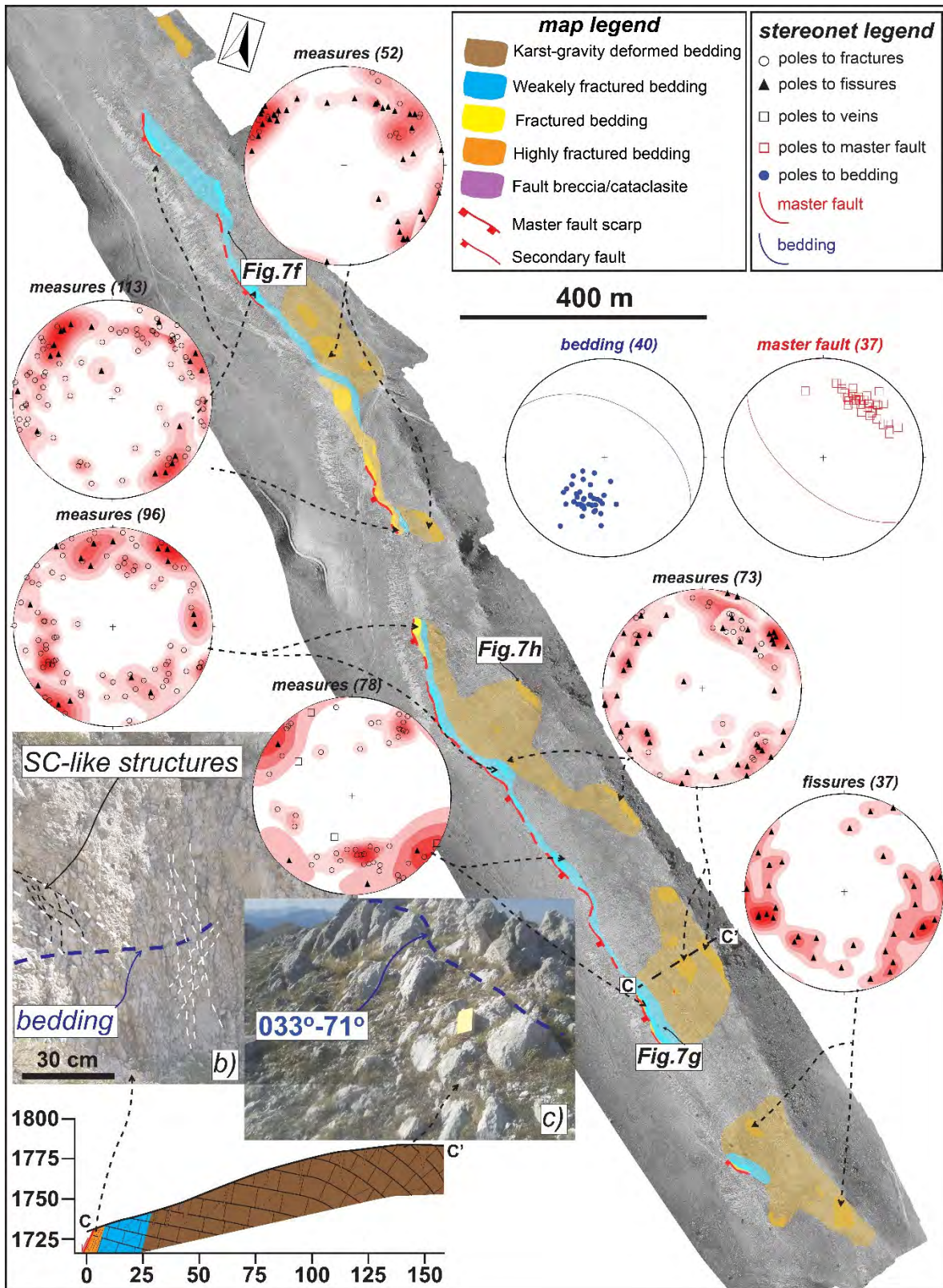
443 across the fault zone and structural data collected within the different structural units, plotted in Equal Area-Lower

444 Hemisphere stereonet with density contours areas (see figure legend for symbols description). The inferred distribution

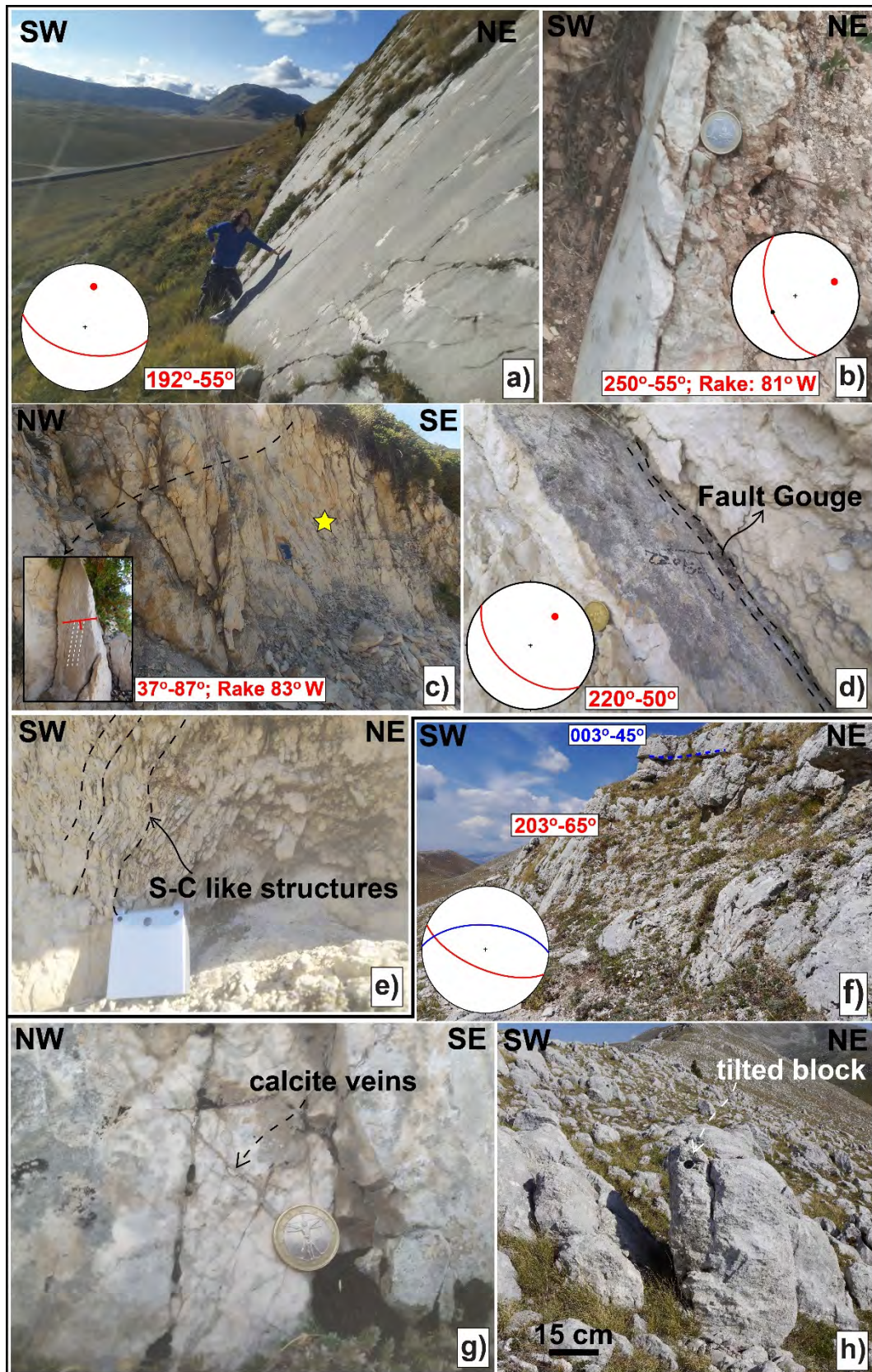
445 of the structural units was drawn with higher degree of transparency. b) Detail of a large secondary fault affecting the

446 host rocks in Fractured rocks domains, with a fault crush breccia associated.

447



448
 449 Figure 6: Structural map of the Cama fault zone, cross section (NE oriented) across the fault zone and structural data
 450 collected within the different structural units, plotted in Equal Area-Lower Hemisphere stereonet with density contours
 451 areas (see figure legend for symbols description). The inferred distribution of the structural units was drawn with higher
 452 degree of transparency. b) Highly fractured rocks located close to the master fault scarp, with fractures spaced < 3 cm
 453 apart and arranged in several sets, locally forming S-C like structures. c) Carbonate host rocks located close to the hill
 454 crest, dipping at high angles and affected by large fissures with 2-30 cm of aperture.



455

456

457

458

459

Figure 7. Main structural elements observed in the Campo Felice and Cama fault zones. a) Campo Felice fault scarp along the Mt. Cefalone, reaching the maximum height of ~ 15 m. b) Polished Campo Felice fault surface affecting the bauxites (Sample CF22_P). c) Cataclastic fault core in between a step-over zone affected by numerous secondary faults with polished slip surfaces showing a dip-slip kinematics (Star indicates the location of Sample CF05). d) Large

460 secondary fault with gouge associated, dipping synthetically with the master fault. e) S-C like structures in Highly
461 fractured volumes across the Campo Felice fault zone. f) Cama fault scarp sharply cutting NE dipping carbonate rocks.
462 g) Small and thin calcite veins, conjugated themselves, affecting the karstified Cama fault surface. h) Blocks of
463 carbonate host rocks close to the hillcrest top cracked and tilted down to the slope. Red and blue lines in the stereoplot
464 indicate the fault and bedding attitude, respectively. WGS84 GPS Location: 42.227594°N, 13.445696°E (a);
465 42.212690°N, 13.466460°E (b); 42.223827°N, 13.454746°E (c); 42.234210°N, 13.437396°E (d); 42.227505°N,
466 13.447607°E (e); 42.274730°N, 13.411760°E (f); 42.275030°N, 13.411420°E (g); 42.278070°N, 13.408900°E (h).

467
468
469

470 4.3 Microstructures of the slip zones

471 In this section, we describe the microstructures of the slip zones of the Campo Felice and Cama
472 faults following the classification of Sibson (1977, 2003). We define as slip surface the exposed fault
473 surface, either polished or karstified. We indicate as slip zone the deformed rocks located beneath the
474 slip surface (up to several centimeters thick) that accommodate the shear strain produced during fault
475 slip (Chester and Chester, 1998; Sibson, 2003). Where present, Principal Slip Zones (PSZs) consist
476 of texturally distinct layers, usually few mm thick, located immediately beneath the slip surface, that
477 accommodate most of the fault displacement (Smith et al., 2011).

478

479 4.3.1. Slip zones of the Campo Felice Fault Zone

480 The slip zone associated with the Campo Felice master fault surface (mostly rough, due to karst-
481 erosional processes) has a proto-cataclastic fabric consisting of angular to sub-rounded fragments of
482 the host rocks (1-5 mm thick) surrounded by a fine matrix (white or reddish in the field and dark grey
483 or brownish under the OM; Fig. 8a). Moving toward the slip surface, the fabric becomes more
484 cataclastic, as the amount of fine matrix increases up to > 50% of the total volume (Fig. 8a). The
485 fragments are cut by numerous shear fractures (< 0.5 mm thick) oriented sub-parallel (i.e., Y-shear
486 fractures) or up to ~ 40° with respect to the slip surface (i.e., P-shear fractures). Some of them are
487 filled with calcite (see black arrows), oxides or clay minerals (Fig. 8a-d). Where clay minerals and
488 oxides are abundant, the texture of fine matrix is composed of calcite micro-grains with irregular to

489 stylolitic-like boundaries, commonly indented and forming incipient triple junctions, with numerous
490 pore spaces locally filled with clay minerals (Fig. 8b, c). Where the fault surface is locally preserved
491 along-strike by sub-aerial exposure, the slip surface is very smooth and has a sharp contact with the
492 underlying clasts (Fig. 8e). The slip zone is a well-developed cataclasite composed of millimetres to
493 centimetres in size sub-angular fragments cut and locally rimmed by thin veins filled by sparite and
494 oxides (white arrows in Fig. 8e).

495 The minor secondary faults affecting the fault core in the step over zones have a very smooth
496 slip surface and a slip zone made of angular to sub-rounded fragments. The latter are 2-8 mm in size,
497 are internally fractured and are immersed in a dark fine matrix (< 50% of the total volume; Fig. 8f).
498 The slip zone includes also a ~ 1-2-mm-thick discontinuous ultra-cataclastic layer close to the slip
499 surface, made of > 90% of fine matrix surrounding few rounded clasts (< 0.5 mm in size; Fig. 8f).
500 The matrix shows a foam-like fabric consisting of sub-euhedral micrometric to nanometric in size
501 calcite grains with straight boundaries, forming triple and quadruple junctions and few pore spaces
502 (Fig. 8g).

503

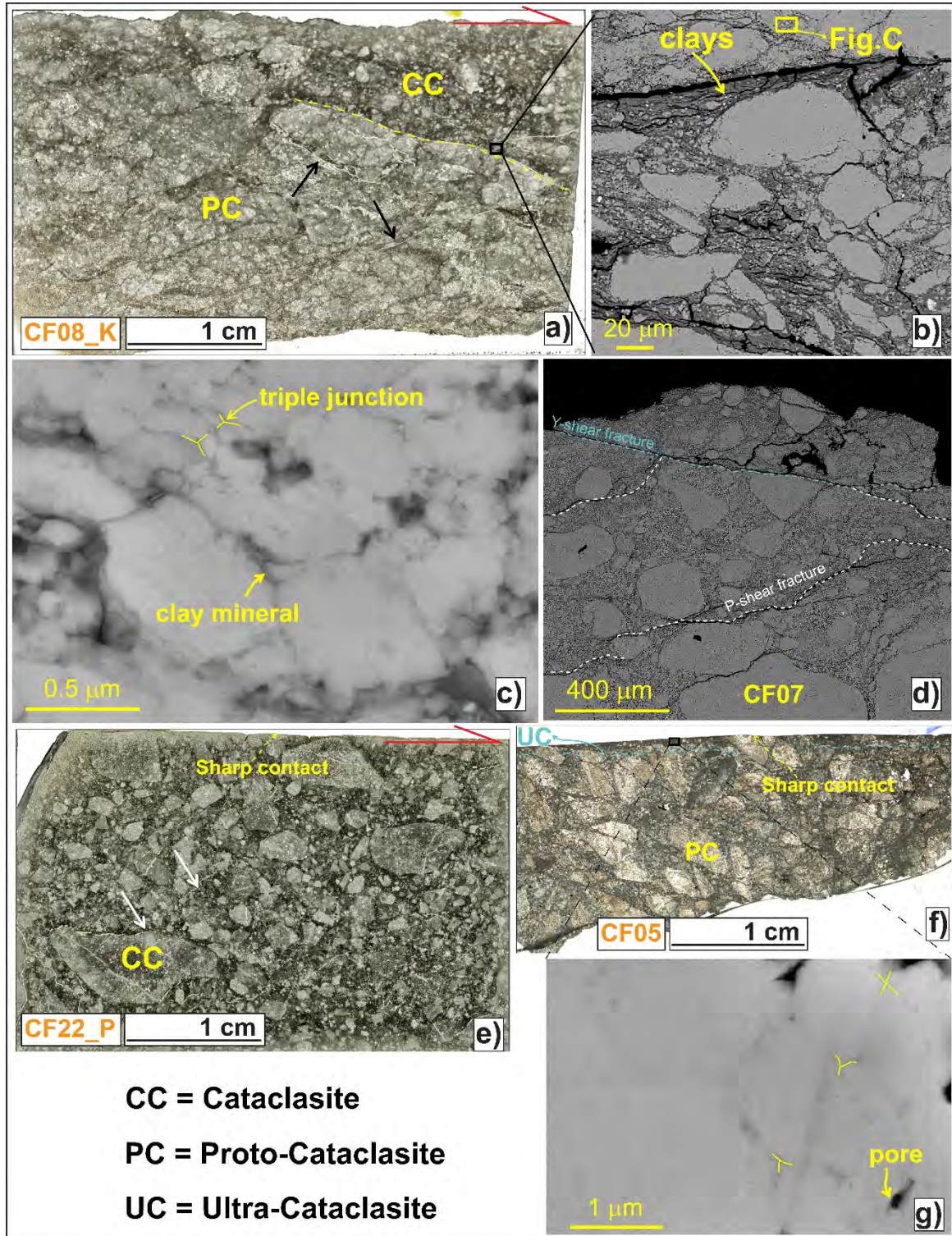
504 4.3.2. Slip zones of the Cama Fault Zone

505 The fault rock close to the Cama fault surface is a chaotic to mosaic breccia (Woodcock and
506 Mort, 2008) composed of incipient angular clasts (1-10 mm in size) cut by numerous fractures
507 oriented 50°-90° to the slip surface (very rough due to karst processes) and forming conjugated pairs
508 (Fig. 9a). Most fractures are filled with secondary sparite, composed of blocky and almost euhedral
509 calcite grains (Bons et al., 2012), with straight and indented (white in color arrows in Fig. 9d)
510 boundaries (Fig. 9c-d).

511 In the few and small (i.e., 2-5 m along-strike) areas where the intensity of damage increases
512 along the fault scarp, the slip zone consists of < 1 mm to 5 mm in size sub-angular clasts surrounded
513 by a brownish fine matrix (Fig. 9b). The slip zone includes numerous pores and fractures oriented
514 both at high-angle and parallel to the slip surface, rarely filled with calcite, and thin convoluted layers

515 close to the top. Overall, this fabric is quite similar to the one observed in the slip zone of the Campo
 516 Felice fault (Fig. 8a-e).

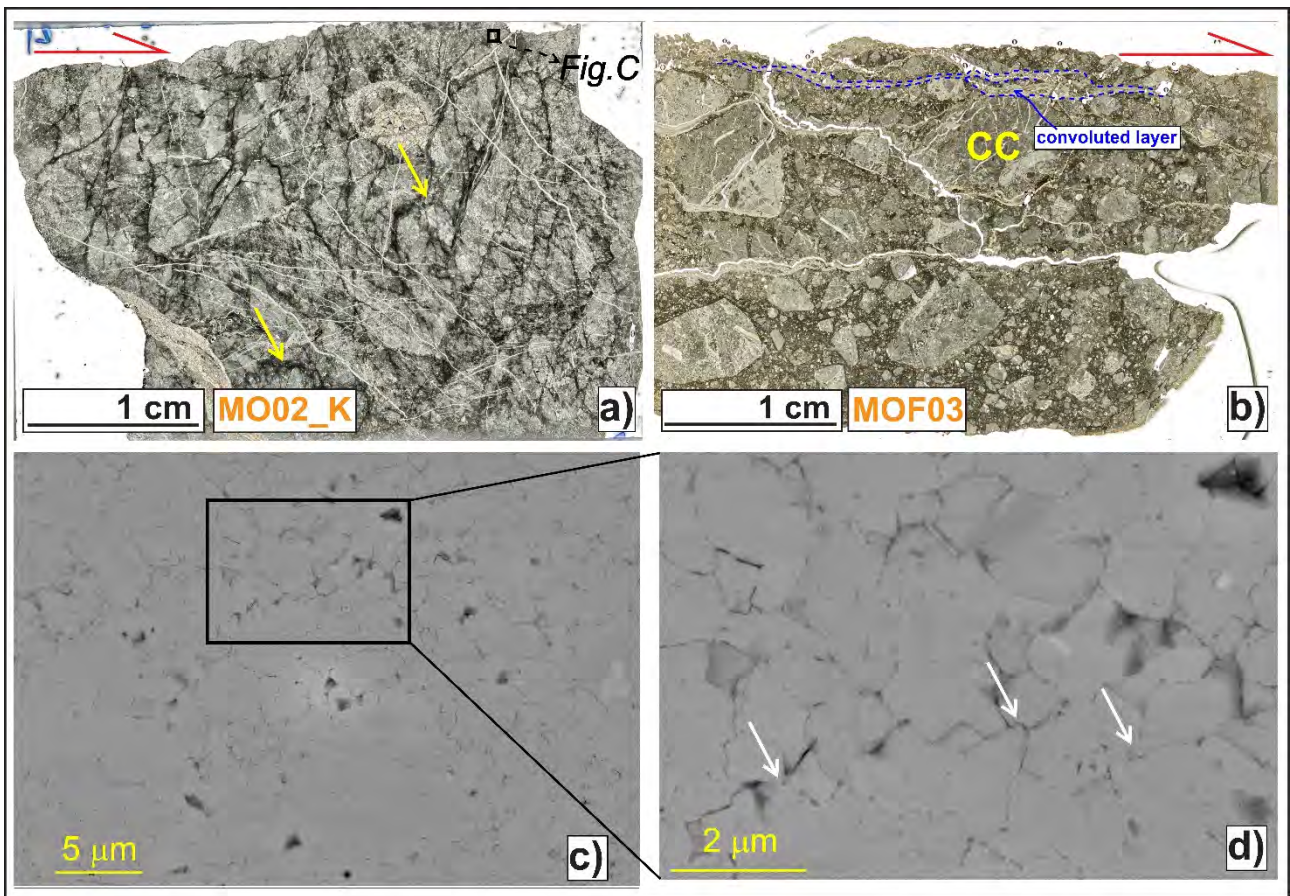
517



518

519 Figure 8. Microstructures of the slip zones of the Campo Felice fault zone. a) Slip zone associated with the master fault
 520 surface (quite rough), showing a proto-cataclastic to cataclastic fabric made of angular to sub-rounded host rock
 521 fragments (1-5 mm thick) immersed in a fine grey matrix and cut by <0.5-mm-thick fractures filled with calcite (black

522 arrows). b-c) Clay minerals filling the fracture spaces and surrounding the calcite grains. The latter shows stylolitic-like
 523 boundaries and from incipient triple junctions. d) Y-shear and P-shear fractures close to the slip surface. e) Well-
 524 preserved slip surface, very smooth and with a net contact with the calcite fragments, partially rimmed by < 0.5-mm-
 525 thick calcite veins (black arrows). f) Slip zone of a well-preserved minor fault including a discontinuous ultra-
 526 cataclastic layer (i.e., PSZ) close to the polished slip surface, that has a net contact with the calcite fragments. g) Matrix
 527 of the PSZ, composed of sub-euhedral calcite grains with straight boundaries, forming well-developed triple and
 528 quadruple junctions. WGS84 GPS Location: 42.227594°N, 13.445696°E (a, b, c, d); 42.212690°N, 13.466460°E (e);
 529 42.223827°N, 13.454746°E (f, g);
 530



531
 532 Figure 9. Microstructures of the Cama fault slip zone. a) The slip zone consists of chaotic to mosaic breccias composed
 533 of < 1 cm in size angular clasts, cut by numerous fractures oriented at high angles with the very rough slip surface,
 534 locally filled with sparite. b) Slip zone where the intensity of fractures increases, showing a cataclastic fabric composed
 535 of sub-angular clasts with different size surrounded by a fine matrix and cut by large fractures oriented both at high-
 536 angles and parallel to the slip surface (very rough due to karst processes). c-d) Blocky calcite grains filling the fracture
 537 spaces, with straight to indented boundaries (white arrows). WGS84 GPS Location: 42.275030°N, 13.411420°E (a, c,
 538 d); 42.283250°N, 13.398110°E (b).
 539
 540
 541
 542

5. Discussion

543 In section 5.1 we discuss the structural features associated with the Campo Felice and Cama normal
544 fault zones, affecting the same carbonate rocks with different cumulated throws (Table 1). In section
545 5.2 we interpret the main the deformation mechanisms active during sliding in the fault slip zones
546 (Table 1). Geomorphological evidence supporting the hypothesis that currently the Cama normal fault
547 represents the upper emergence of the shear zone associated with the lateral spreading (DSGD) of
548 Mt. D'Ocre Range is also discussed. In fact, as in the typical case of laterally spreading DGSDs, the
549 basal shear zone does not crop out (Varnes, 1978; Hutchinson, 1988; Agliardi et al., 2001, 2012;
550 Crosta et al., 2013; Dramis and smile-valvo, 1994; Discenza et al., 2021).

551

552 5.1 Meso-structural proprieties of the Campo Felice and Cama faults

553 The Campo Felice fault has an almost continuously exposed sharp fault scarp ~ 3-4-m-high on
554 average, up to 15 m in some areas (e.g., Fig. 7a), locally undulated along-strike (Figs. 4-5). The fault
555 core decorates the fault scarp for several kilometres and mainly consists of cataclasites (~ 0-40 cm in
556 thickness) and crush fault breccias (50-cm to 2 m in thickness). The latter are cut by calcite veins and
557 several sub-vertical secondary faults dipping both synthetically and antithetically with the master
558 fault and controlling the heterogeneous distribution of the different structural units forming the
559 footwall damage zones (Fig. 3b-e). In particular, Highly fractured and fractured rock volumes are
560 spatially associated with secondary faults. In these domains, most of the fractures are spaced < 3 cm
561 and 3-10 cm apart and steeply dipping, with orientation consistent with the one of the secondary faults
562 and with the ongoing NE-SW oriented Pleistocene regional extension (Ferrarrini et al., 2015;
563 Lavecchia et al., 1994). The fault is composed of numerous segments arranged in *én-echelon* step-
564 over zones, where the fault core is wider (i.e., up to 15-m-thick) and fracture intensity strongly
565 increases, thus favoring the infiltration of meteoric waters and the development of stylolites and S-C
566 like structures (Figs. 3a, 6c-d, 7e). Such structural features were also observed in other large-
567 displacement normal faults in the central Apennines (e.g., San Benedetto-Gioia dei Marsi fault

568 segment, Agosta and Aydin, 2006; Campo Imperatore fault system, Fondriest et al., 2020; Demurtas
569 et al., 2016) although these faults have wider fault cores (i.e., 1 to 40 m thick) and damage zones (up
570 to several hundred meters thick).

571 Instead, the architecture of the Cama fault is less structurally developed compared with the one
572 of Camo Felice fault. The fault scarp is discontinuous and crops out only in the middle and southern
573 sectors, with maximum height of ~ 2 m. The fault core is almost absent, except close to the south-
574 eastern tip, where it consists of mosaic fault breccias (Woodcock and Mort, 2008) and the damage
575 zone is < 40-m-thick and not affected by secondary faults (Fig. 6). Extensional fractures are usually
576 spaced > 10 cm apart, except in few areas close to the master fault, where they are spaced < 3 cm
577 apart and conjugated themselves (Fig. 6) with orientation consistent with the Pleistocene extensional
578 phase. These architectural features are typical of immature/incipient or small-displacement faults
579 (Faulkner et al., 2011; Savage and Brodsky, 2011; Mayolle et al., 2019) and would be consistent with
580 the ~ 100 m of maximum geological throw (cross-section B-B'; Fig. 2d) and low Quaternary throw
581 rates estimated (0.2 mm/yr; Salvi et al., 2003).

582 This interpretation would be also confirmed by the absence of wide (i.e., tens of kms²)
583 Quaternary basins associated with the Monte D'Ocre faults, that instead border small and narrow (i.e.,
584 < 400 m wide; Figs. 1, 2, 6) valleys to SW. Indeed, large Quaternary basins are commonly associated
585 with tens of km-long active normal faults, especially in central Apennines (Bosi et al., 2003), where,
586 however, some basins could have been inherited from the compressional stage (e.g., in between
587 nearby thrusts) and not directly produced by the bounding normal faults (Mancinelli et al., 2021).

588 Nevertheless, several sub-vertical fissures affect the host rocks in the footwall of the Cama fault.
589 Average fracture/fissure aperture increases from 10-15 cm to > 20 cm (up to 1 m) toward the hillcrest
590 top, also favored by dissolution associated to karst processes, that are very efficient in calcite-built
591 rocks especially at low ambient temperature (Andriani and Parise, 2015). Here, the relatively high
592 potential relief promotes the formation of gravitational trenches, that are commonly associated with
593 tilted blocks at the surface (Figs. 3a, 7h). Other landforms typically associated with gravitational

594 processes, such as double-crested lines, up-hill and down-hill facing scarps, mainly aligned in the
595 NW-SE direction, shape the Mt. D'Ocre range (see Fig. 2 in Albano et al., 2015; Salvi et al., 2003;
596 Fig. 1). The large fissures affecting the host rocks and associated landforms are consistent with their
597 development in tensional regime (i.e., negative values of minimum principal stress; Del Rio et al.,
598 2021) or at very low confining pressures, with principal stress oriented sub-parallel to the fracture
599 surface (i.e., Mode I fracture; Fossen, 2010). These structural and geomorphological observations
600 suggest that the Cama master fault surface is currently accommodating the lateral spreading of Mt.
601 D'Ocre Range, mainly moving by creep, together with the Campoli-Cerasitto fault and other faults
602 of the area (Figs. 1, 2b, d). Therefore, this fault is not expected to link at depth with the Campo Felice
603 fault, given the large differences in cumulated throw and throw rates (table 1) and the current
604 mechanical behaviors (i.e., tectonic vs. gravitative) and, thus, not represent a segment of the active
605 Ovindoli-L'Aquila Fault System as proposed by other authors (Salvi et al., 2003; Galli et al., 2008).
606 However, given the proximity with the Campo Felice fault, episodic movements along these faults
607 can likely be induced by ground shaking produced by earthquakes (Salvi and Nardi, 1995; Albano et
608 al., 2015), also consistent with the average fault dip angles of $\sim 60^\circ$ (Fig. 5). According to this
609 interpretation, the length of the seismogenic source associated with the Ovindoli-L'Aquila Fault
610 System would be reduced of $\sim 8-9$ km. This, in turn, would result in a lower maximum expected
611 earthquake magnitude (i.e., $M_w \sim 6.5$) associated with the entire re-activation of the fault system (e.g.,
612 Wells and Coppersmith, 1994; Wesnousky, 2008; Leonard, 2010; Galli et al., 2008).

613

614 5.2 Deformation mechanisms of the Campo Felice and Cama fault slip zones

615 In active fault zones, the bulk of displacement cumulated during individual earthquakes is mainly
616 accommodated in the fault core, in particular within highly localized cataclastic mm-cm thick
617 principal slip zones (Power and Tullis, 1989; Chester et al., 1993; Caine et al., 1996; Chester and
618 Chester, 1998; Sibson, 2003; Smith et al., 2011, 2015).

619 The Campo Felice fault surface is quite rough where the exposed fault scarp is karstified (Fig.
620 8a). The associated slip zone shows a proto-cataclastic to cataclastic fabric, including thin calcite
621 veins and both Y-shear and P-shear fractures, but lack of a well-defined ultra-cataclastic layer close
622 to the slip surface (i.e., the PSZ), possibly obliterated by weathering (Fig. 8a, d). Where preserved by
623 surficial alteration, the fault surface is smoother and has a sharp contact with the larger clasts of the
624 underlying cataclastic slip zone (Fig. 8e). The well-preserved slip surfaces of secondary faults are
625 very smooth to polished, with an associated proto-cataclastic/cataclastic slip zone that includes a ~ 1-
626 2-mm-thick ultra-cataclastic PSZ (Fig. 8f). On the contrary, the slip surface of the Cama fault is very
627 rough, in part due to weathering of the exposed fault scarp, and lacks of a neat PSZ. Indeed, the fault
628 rock beneath the slip surface is a chaotic to mosaic fault breccia cut by numerous fractures and calcite
629 veins (0.1-0.2 mm thick) oriented at high-angles (i.e., $> 50^\circ$) with respect to the slip surface (Fig. 9a).

630 The fine matrix surrounding clasts in the Campo Felice master fault core is composed of calcite
631 micro-grains with irregular to stylolitic-like boundaries, pores, incipient triple junctions and
632 indentation structures interpreted as due to pressure-solution processes (Rutter, 1983; Gratier et al.,
633 2013; Fig. 8b, c). Pressure-solution is a water-assisted process mainly driven by the stress acting at
634 the grain-to-grain contacts that occurs through dissolution at grain boundaries, diffusion of the solute
635 matter, and precipitation of the latter within pore spaces (Rutter, 1983; Tada and Siever, 1989; Lehner,
636 1995; Gundersen et al., 2002; Croizè et al., 2013). Pressure-solution processes are locally promoted
637 by the presence of oxides and clay minerals within the pore spaces, that prevent grain boundary
638 healing (Renard et al., 2001), possibly deriving by the smearing of the bauxitic layers cut by the
639 Campo Felice fault.

640 These processes are also controlled by the grain size (Rutter, 1983; Tada and Siever, 1989;
641 Renard et al., 2000). Indeed, in the ultra-cataclastic PSZ, where the average grain size is smaller due
642 to the higher degree of grain comminution, the fine matrix is mainly composed of more packed sub-
643 euahedral calcite grains, with straighter boundaries and more developed triple junctions (Fig. 8g).
644 Pressure-solution processes also favor dissolution and formation of stylolites (Ehrenberg et al., 2006;

645 Aharonov and Katsman, 2009). In the case of Cama fault slip zone, the sub-grains of the fault breccia
646 have irregular to stylolitic boundaries and are affected by numerous veins filled with secondary
647 sparite (Fig. 9a). The latter is composed of sub-euhedral and blocky calcite grains with straight
648 contacts and indentation structures suggesting fluid circulation and rapid precipitation after fracturing
649 at very shallow crustal levels and congruent pressure-solution processes (Fig. 9c, d).

650 Microstructural analyses indicate that similar deformation mechanisms (i.e., cataclasis and
651 pressure-solution) occur in both the Campo Felice and Cama faults. However, the slip zones
652 associated with the two fault scarps have different fabrics (i.e., cataclasite vs. crush fault breccia) and
653 textures of the fine matrix. These differences can be mainly explained by the higher average long-
654 term slip rates and cumulated geological throws of the Campo Felice fault with respect to the Cama
655 fault and also by the higher amount of clay minerals in the Campo Felice slip zone than in the Cama
656 one (see Table 1). Indeed, in the few areas where the intensity of fracture increases along the Cama
657 fault, the slip zone shows a cataclastic fabric quite similar to the one observed in the slip zone of
658 Campo Felice fault (compare Fig. 8a-e, with Fig. 9b).

659

660 Table 1

661 Comparison of the main geological and structural features of the Campo Felice and Cama faults

	Campo Felice fault	Cama fault
<i>Along-strike length</i>	~ 6 km	~ 3 km
<i>Fault scarp height</i>	~ 4 m, up to 15 m	max. 2 m
<i>Max. geol throw</i>	1050 m (error 425 m)	~ 100 m
<i>throw rates</i>	~ 1 mm/yr	0.2 mm/yr
<i>Damage zone thickness</i>	> 400 m	~ 40 m
<i>Core thickness</i>	~ 40 cm, up to 15 m	almost absent
<i>Secondary faults</i>	numerous in both core and damage zone	not found
<i>Veins</i>	numerous in both core and damage zone	only close to the fault scarp and very thin (< 5 mm)
<i>Slip zones microstructures</i>	Cataclasite to Ultra-cataclasite	Crush breccia to cataclasite
<i>Deformation mechanisms</i>	Cataclasis and pressure-solution	Cataclasis and pressure-solution

662

663

664

665

6. Conclusions

666

667

668

669

670

671

672

673

674

675

676

In this work, we compared the Campo Felice and Cama normal fault zones (Table 1). The maximum estimated geological throw of the Campo Felice fault is ~ 1050 m, with a possible overestimate of ~ 400 m (Fig. 2c). The fault scarp (3-15 m high) is continuous along-strike and composed of numerous segments arranged *en-echelon*. The fault core (40 cm to 15 m thick) and highly fractured rocks domains (50-150 m thick and with fractures < 3 cm spaced apart) are cut by numerous high-angle secondary faults and veins (Figs. 4, 5). On the contrary, the Cama fault scarp (~ 2 m high) discontinuously outcrops only in the middle and southern sectors. The fault core is almost absent and fractures in the damage zone (< 40 m thick) are usually spaced > 10 cm apart, consistent with the ~ 100 m of maximum geological throw and the estimated low Quaternary throw rates estimated (Figs. 2d, 6). Furthermore, the numerous high-angle fissures affecting the footwall block and associated gravitative geomorphological structures (e.g., double-crested lines, scarps and

677 counter-slope scarps) are coherent with an immature/incipient and small-displacement normal fault
678 that is currently re-used by gravity to accommodate the lateral spreading of Mt. D'Ocre Ridge.
679 Therefore, the Cama fault is not expected to link at depth with the Campo Felice fault, whose damage
680 zone shows architectural features consistent with what observed in other large-displacement normal
681 fault zones in the central Apennines. According to this interpretation, the seismogenic source
682 associated with the Ovindoli-L'Aquila Fault System would be reduced up to 8-9 km, thus reducing
683 the maximum expected earthquake magnitude of the fault system from ~ 6.8 to ~ 6.5 (Wells and
684 Coppersmith, 1994). However, the possible reduction of the seismogenic potential of the Ovindoli-
685 L'Aquila Fault System is based on the hypothesis that the Cama fault is currently the shear zone of a
686 laterally spreading DSGD and not linked at depth with the Campo Felice fault (Fig. 1d). Since in
687 laterally spreading DGSDs the basal shear zone usually does not crop out (Varnes, 1978; Hutchinson,
688 1988; Agliardi et al., 2001, 2012; Crosta et al., 2013; Dramis and smile-valvo, 1994; Discenza et al.,
689 2021) this hypothesis requires further geophysical investigations. Nevertheless, recent throw
690 distribution and structural field analyses suggest a possible shallow soft-linkage to NW between the
691 Campo Felice and Mt. Orsello faults (Fig. 1; Spagnolo et al., 2021).

692
693 The slip zone of the Campo Felice fault is a proto-cataclasite to cataclasite composed of angular
694 to sub-rounded clasts (1-5 mm thick) surrounded by a fine matrix whose amount increases toward the
695 slip surface (Fig. 8a). On the contrary, the slip zone of Cama fault is a mosaic breccia with 1-10 mm
696 thick angular clasts cut by numerous fractures filled with sparite (Fig. 9a). The fine matrix of the
697 Campo Felice fault slip zone is composed of calcite micro-grains with irregular to stylolitic-like
698 boundaries and pores locally filled with oxides and clay minerals, with incipient triple junctions and
699 indentation structures, interpreted as due to pressure-solution processes. Instead, the secondary sparite
700 filling the fractures of the Cama fault slip zone is composed of blocky calcite grains, locally indented,
701 with straight to irregular boundaries, due to rapid precipitation after fracturing at shallow crustal
702 levels and pressure-solution processes (Fig. 9c, d). Such observations indicate how in carbonate-

703 hosted normal faults, cataclasis and pressure-solution processes are the main deformation
704 mechanisms active during sliding. These processes are much more active in the case of Campo Felice
705 fault because of the larger displacement cumulated in time and amount of clay minerals with respect
706 to the Cama fault, that allowed for a much higher grain comminution and lower grain boundary
707 healing enhancing pressure-solution processes.

708 This work shows how the systematic study at meso- to micro-scale of fault zones can be
709 integrated with geomorphological and geological analyses to provide further parameters to improve
710 the characterization of seismogenic sources (Galadini et al., 2012; Falcucci et al., 2016).

711

712 **Acknowledgments**

713 This research was funded by the European Research Council Consolidator Grant Project NOFEAR
714 No 614705 (L.D.R., M.F. and G.D.T.), by the INGV projects: “*Caratterizzazione microstrutturale*
715 *di piani di faglia attivi ed esumati e di piani di scivolamento di deformazioni gravitative profonde*
716 *di versante (DGPV)*” and “Investigation of bedrock shear planes microstructures” and by a Marie
717 Curie Fellowship (M.M.). S.M. acknowledges Fondazione CARIPARO for funding his PhD
718 scholarship. We thank Leonardo Tauro for thin section preparation, Nicola Michelon for preparing
719 field materials and thin section scans and Girolamo Dixit Dominus for support in field work.
720 Fabrizio Agosta, Andrea Billi and an anonymous Reviewer are thanked for their constructive
721 comments.

722

723 **Author contributions**

724 M.M., M.S., G.D.T. and L.D.R. conceived the original idea; F.D. drone imaging; L.D.R., S.M.,
725 M.M., and G.D.T. field work; L.D.R. and A.C. microstructural analyses; L.D.R., G.D.T. and S.M.,
726 microstructural interpretation; L.D.R. wrote the manuscript with input from G.D.T., M.M., F.D., S.
727 M. All authors discussed the results and commented on the manuscript.

728

729 **Data Availability statement**

730 None of the data in our manuscript have been published or are under consideration elsewhere. The
731 collected data set was uploaded and is available on <http://researchdata.cab.unipd.it/id/eprint/672>
732 (DOI: [10.25430/ researchdata.cab.unipd.it.00000672](https://doi.org/10.25430/researchdata.cab.unipd.it.00000672)).

733

734 **References**

- 735 Agliardi, F., Crosta, G., Zanchi, A., 2001. Structural constraints on deep-seated slope deformation
736 kinematics. *Engineering Geology*, 59, 83–102. [https://doi.org/10.1016/s0013-7952\(00\)00066-](https://doi.org/10.1016/s0013-7952(00)00066-1)
737 [1](https://doi.org/10.1016/s0013-7952(00)00066-1)
- 738 Agliardi, F., Crosta, G., Frattini, P., 2012. Slow rock-slope deformation. In: Clague, J.J., Stead, D.
739 (Eds.), *Landslides Types, Mechanisms and Modeling*, pp. 207-221. Cambridge: Cambridge
740 University Press.
- 741 Agosta, F., Aydin, A., 2006. Architecture and deformation mechanism of a basin bounding normal
742 fault in Mesozoic platform carbonates, central Italy. *Journal of Structural Geology*, 28(8),
743 1445–1467. <https://doi.org/10.1016/j.jsg.2006.04.006>
- 744 Aharonov, E., Katsman., R., 2009. Interaction between pressure solution and clays in stylolite
745 development: Insights from modeling, *American Journal of Science*, 309 (7), 607-632.
- 746 Albano, M., Barba, S., Saroli, M., Moro, M., Malvarosa, F., Costantini, M., Bignami, C.,
747 Stramondo, S., 2015. Gravity-driven postseismic deformation following the Mw 6.3 2009
748 L’Aquila (Italy) earthquake. *Sci. Rep.* 5, 16558.
- 749 Allmendinger, R.W., Cardozo, N., Fisher, D., 2011. *Structural geology algorithms: Vectors and*
750 *tensors*. Cambridge University Press.
- 751 Andriani G.F., Parise M., 2015. On the applicability of geomechanical models for carbonate rock
752 masses interested by karst processes. *Environ Earth Sciences*, this special issue
- 753 Billi, A., Salvini, F., Storti, F., 2003. The damage zone-fault core transition in carbonate rocks:
754 implications for fault growth, structure and permeability. *J. Struct. Geol.*, 25 1779-1794.

755 Boncio, P., Lavecchia, G., Pace, B., 2004. Defining a model of 3D seismogenic sources for seismic
756 hazard assessment applications: The case of central Apennines (Italy). *Journal of Seismology*.
757 8(3), 407–425. <https://doi.org/10.1023/b:jose.0000038449.78801.05>.

758 Bons, P.D., Elburg, M.A., Gomez-Rivas, E., 2012. A review of the formation of tectonic veins and
759 their microstructures. *J. Struct. Geol.* 43, 33–62. <https://doi.org/10.1016/j.jsg.2012.07.005>.

760 Bosi, C., Galadini, F., Messina, P., 1993. Neotectonic significance of bedrock fault scarps: case
761 studies from the Lazio-Abruzzi Apennines (central Italy). *Z. Geomorphol., Suppl.*bd. 94, 187-
762 206.

763 Bosi, C., Galadini, F., Giaccio, B., Messina, P., Sposato, A., 2003. Plio-Quaternary continental
764 deposits in the Latium-Abruzzi Apennines: The correlation of geological events across
765 different intermontane basins. *Il Quaternario*, 16, 55–76.

766 Bozzano F., Bretschneider A., Esposito C., Martino S., Prestininzi A., Scarascia Mugnozza G.,
767 2013. - lateral spreading processes in mountain ranges: insights from an analogue modelling
768 experiment. *tectonophysics*, 605: 88-95. <https://doi.org/10.1016/j.tecto.2013.05.006>

769 Brandano, M., 2017. Unravelling the origin of a Paleogene unconformity in the Latium-Abruzzi
770 carbonate succession: A shaved platform. *Palaeogeography, Palaeoclimatology,*
771 *Palaeoecology* 485: 687– 696.

772 Caine, J.S., Evans, J.P., Forster, C.B., 1996. Fault zone architecture and permeability structure.
773 *Geology*, 24(11), 1025–1028. [https://doi.org/10.1130/00917613\(1996\)](https://doi.org/10.1130/00917613(1996)).

774 Cardozo, N., Allmendinger, R.W., 2013. Spherical projections with OSX Stereonet. *Comput.*
775 *Geosci.*, 51, 193-205, [10.1016/j.cageo.2012.07.021](https://doi.org/10.1016/j.cageo.2012.07.021)

776 Carminati, E., Doglioni, C., 2012. Alps vs. Apennines: The paradigm of a tectonically asymmetric
777 Earth. *Earth-Science Reviews*, 112(1–2), 67–96.
778 <https://doi.org/10.1016/j.earscirev.2012.02.004>

779 Carminati, E., Lustrino, M., Doglioni, C., 2012. Geodynamic evolution of the central and western
780 Mediterranean: Tectonics vs. igneous petrology constraints. *Tectonophysics*, 579, 173–192.
781 <https://doi.org/10.1016/j.tecto.2012.01.026>

782 Cavinato, G.P., Carusi, C., Dall'Asta, M., Miccadei, E., Piacentini, T., 2002. Sedimentary and
783 tectonic evolution of Plio-Pleistocene alluvial and lacustrine deposits of the Fucino Basin
784 (central Italy). *Sedimentary Geology*, 148, 29–59. [https://doi.org/10.1016/s0037-](https://doi.org/10.1016/s0037-0738(01)00209-3)
785 [0738\(01\)00209-3](https://doi.org/10.1016/s0037-0738(01)00209-3).

786 Chester, F.M., Logan, J.M., 1986. Implications for mechanical properties of brittle faults from
787 observations of the Punchbowl fault zone, California. *Pure Appl. Geophys.* 124, 79–106.

788 Chester, F.M., Biegel, R.L., Evans, J.P., 1993. Internal structure and weakening mechanisms of the
789 San-Andreas fault. *J. Geophys. Res: Solid Earth*, 98, 771-786.

790 Chester, F.M., Chester, J.S., 1998. Ultracataclasite structure and friction processes of the
791 Punchbowl fault, San Andreas system, California. *Tectonophysics*, 295, 199–221.
792 [https://doi.org/10.1016/s0040-1951\(98\)00121-8](https://doi.org/10.1016/s0040-1951(98)00121-8).

793 Chiaraluce, L., Di Stefano, R., Tinti, E., Scognamiglio, L., Michele, M., Casarotti, E., et al.,
794 2017. The 2016 Central Italy seismic sequence: A first look at the mainshocks, aftershocks,
795 and source models. *Seismological Research Letters*, 88(3), 757-
796 771. <https://doi.org/10.1785/0220160221>

797 Choi, J.H., Edwards, P., Ko, K., Kim, Y.S., 2016. Definition and classification of fault damage
798 zones: a review and a new methodological approach. *Earth-Sci. Rev.*, 152, 70-87.

799 Clemenzi L., Storti F., Balsamo F., Molli G., Ellam R., Mucchez P., Swenne R., 2015. Fluid pressure
800 cycles, variations in permeability, and weakening mechanisms along low-angle normal faults:
801 the Tellaro detachment, Italy. *Geol. Soc. Am. Bull.*, 127 (11–12), 1689-1710.

802 Cosentino, D., Cipollari, P., Marsili, P., Scrocca D., 2010. Geology of the Central Apennines: a
803 regional review *J. Virtual Explor.* 36, 1-37.

804 Croizè, D., Renard, F., Gratier, J.P., 2013. Compaction and porosity reduction in carbonates: A
805 review of observations, theory, and experiments. *Advances in Geophysics*, 54, 181–238.
806 <https://doi.org/10.1016/b978-0-12-380940-7.00003-2>.

807 Crosta, G.B., Frattini, P., Agliardi, F., 2013. Deep seated gravitational slope deformations in the
808 European Alps. *Tectonophysics*, 605, 13–33. <https://doi.org/10.1016/j.tecto.2013.04.028>

809 D'Agostino, N., Giuliani, R., Mattone, M., Bonci, L., 2001. Active crustal extension in the central
810 Apennines (Italy) inferred from GPS measurements in the interval 1994-1999. *Geophysical*
811 *Research Letters*, 28, 2121–2124. <https://doi.org/10.1029/2000gl012462>

812 Damiani, A.V., Chiocchini, M., Colacicchi, R., Mariotti, G., Parotto, M., Passeri, L., Praturlon, A.,
813 1992. Elementi litostratigrafici per una sintesi delle facies carbonatiche meso-cenozoiche
814 dell'Appennino centrale. *Studi Geologici Camerti*, vol. spec., 1991/2, 187-213.

815 Del Rio, L., Moro, M., Fondriest, M., Saroli, M., Gori, S., Falcucci, E., Cavallo A., Doumaz, F., Di
816 Toro, G., 2021. Active faulting and deep-seated gravitational slope deformation in carbonate
817 rocks (central Apennines, Italy): A new “close-up” view. *Tectonics*, 40.
818 <https://doi.org/10.1029/2021TC006698>.

819 Demangeot, J., 1965. *Géomorphologie des Abruzzes Adriatiques* (Numero hors serie, Vol.403).
820 Centre Recherche et Documentation Cartographiques Memoires et Documents.

821 Demurtas, M., Fondriest, M., Balsamo, F., Clemenzi, L., Storti, F., Bistacchi, A., Di Toro, G., 2016.
822 Structure of a normal seismogenic fault zone in carbonates: The Vado di Corno fault, Campo
823 Imperatore, central Apennines (Italy). *J. Struct. Geol.*, 90, 185–206.
824 <https://doi.org/10.1016/j.jsg.2016.08.004>

825 Di maggio C., Madonia G., Vattano M., 2014. deep-seated gravitational slope deformations in
826 western sicily: controlling factors, triggering mechanisms, and morphoevolutionary models.
827 *Geomorphology*, 208: 173-189. <https://doi.org/10.1016/j.geomorph.2013.11.023>

828 Di Toro, G., Pennacchioni, G., 2005. Fault plane processes and mesoscopic structure of a strong-
829 type seismogenic fault in tonalites (Adamello batholith, Southern Alps). *Tectonophysics*,
830 402(1–4), 55–80. <https://doi.org/10.1016/j.tecto.2004.12.036>.

831 Discenza, M.E., Esposito, C., 2021. State-of-art and remarks on some open questions about
832 DSGSDs: Hints from a review of the scientific literature on related topics. *Italian Journal of*
833 *Engineering Geology and Environment*, 21 (1), 31-59.

834 Dramis, F., 1983. Morfogenesi di versante nel Pleistocene superiore in Italia: i depositi detritici
835 stratificati. *Geogr. Fis. Din. Quat.* 6, 180– 182.

836 Dramis, F., 1992. Il ruolo dei sollevamenti tettonici a lungo raggio nella genesi del rilievo
837 appenninico. *Studi Geologici Camerti*, vol. spec., 1992/1, 9-15.

838 Dramis, F., Sorriso-Valvo, M., 1994. Deep-seated gravitational slope deformations, related
839 landslides and tectonics. *Engineering Geology*, 38, 231–243. [https://doi.org/10.1016/0013-](https://doi.org/10.1016/0013-7952(94)90040-x)
840 [7952\(94\)90040-x](https://doi.org/10.1016/0013-7952(94)90040-x)

841 Ehrenberg, S.N., McArthur, J.M., Thirlwall, M. F., 2006. Growth, demise, and dolomitization of
842 miocene carbonate platforms on the Marion Plateau, o_shore NE Australia, *Journal of*
843 *Sedimentary Research*, 76 (1), 91-116.

844 Engelder, T., 1987. Joints and shear fractures in rock. In B. K. Atkinson (Ed.), *Fracture mechanics*
845 *of rock* (pp. 27–69). Academic Press. <https://doi.org/10.1016/b978-0-12-066266-1.50007-7>

846 Elter, P., Giglia, G., Tongiorgi, M., Trevisan, L., 1975. Tensional and compressional areas in the
847 recent (Tortonian to present) evolution of the Northern Apennines. *Bollettino di Geofisica*
848 *Teorica ed Applicata*, 17, 3-18.

849 EMERGEIO Working Group (2010). Evidence for surface rupture associated with the MW 6.3
850 L'Aquila earthquake sequence of April 2009 (central Italy). *Terra Nova*, 22(1), 43–51.
851 <https://doi.org/10.1111/j.1365-3121.2009.00915.x>

852 Falcucci, E., Gori, S., Galadini, F., Fubelli, G., Moro, M., Saroli, M., 2016. Active faults in the
853 epicentral and mesoseismal Ml 6.0 24, 2016 Amatrice earthquake region, central Italy.

854 Methodological and seismotectonic issues. *Annals of Geophysics*, 59. <https://doi.org/10.4401/>
855 [ag-7266](https://doi.org/10.4401/ag-7266).

856 Faulkner, D.R., Lewis, A.C. Rutter, E.H., 2003. On the internal structure and mechanics of large
857 strike-slip faults: field observations from the Carboneras fault, southeastern
858 Spain. *Tectonophysics* 367, 235–251.

859 Faulkner, D.R., Jackson, C.A.L., Lunn, R.J., Schlische, R.W., Shipton, Z.K., Wibberley, C.A.J.,
860 Withjack M.O., 2010. A review of recent developments concerning the structure, mechanics
861 and fluid flow properties of fault zones, *J. Struct. Geol.*, 32(11), 1557–1575,
862 doi:10.1016/j.jsg.2010.06.009.

863 Faulkner, D.R., Mitchell, T.M., Jensen, E., Cembrano, J., 2011. Scaling of fault damage zones with
864 displacement and the implications for fault growth processes. *J. Geophys. Res.*, 116 (2011),
865 Article B05403, [10.1029/2010JB007788](https://doi.org/10.1029/2010JB007788)

866 Ferraro, F., Grieco, D. S., Agosta, F., Prosser, G., 2018. Space-time evolution of cataclasis in
867 carbonate fault zones. *Journal of Structural Geology*, 110, 45-64.

868 Ferraro, F., Agosta, F., Ukar, E., Grieco, D. S., Cavalcante, F., Belviso, C., Prosser, G., 2019.
869 Structural diagenesis of carbonate fault rocks exhumed from shallow crustal depths: An
870 example from the central-southern Apennines, Italy. *Journal of Structural Geology*, 122, 58-
871 80.

872 Ferraro, F., Agosta, F., Prasad, M., Vinciguerra, S., Violay, M., Giorgioni, M., 2020. Pore space
873 properties in carbonate fault rocks of peninsular Italy. *Journal of Structural Geology*, 130,
874 103913.

875 Ferrarrini, F., De Nardis, R., Lavecchia, G., Brozzetti, F., 2015. Fault geometry and active stress
876 from earthquakes and field geology data analysis: The Colfiorito 1997 and L'Aquila 2009
877 cases (Central Italy). *Pure and Applied Geophysics*, 172(5), 1079–1103.
878 <https://doi.org/10.1007/s00024-014-0931-7>

879 Fondriest, M., Balsamo, F., Bistacchi, A., Clemenzi, L., Demurtas, M., Storti, F., Di Toro, G., 2020.
880 Structural complexity and mechanics of a shallow crustal seismogenic source (Vado di Corno
881 Fault Zone, Italy). *Journal of Geophysical Research: Solid Earth*, 125. [https://](https://doi.org/10.1029/2019JB018926)
882 doi.org/10.1029/2019JB018926

883 Fossen, H., 2010. *Structural geology* (p. 463). Cambridge University Press.

884 Fossen, H., Rotevatn, A., 2016. Fault linkage and relay structures in extensional settings—a review.
885 *Earth Sci. Rev.* 154, 14-28, [10.1016/j.earscirev.2015.11.014](https://doi.org/10.1016/j.earscirev.2015.11.014)

886 Galadini, F., Galli, P., 2000. Active tectonics in the central Apennines (Italy)—Input data for
887 seismic hazard assessment. *Natural Hazards*. 22, 225–268.
888 <https://doi.org/10.1023/a:1008149531980>.

889 Galadini, F., Galli, P., 2003. Paleoseismology of silent faults in the central Apennines (Italy): the
890 Mt. Vettore and Laga Mts. Faults. *Ann. Geophys.* 46, 815–836.

891 Galadini, F., 2006. Quaternary tectonics and large-scale gravitational deformations with evidence of
892 rock-slide displacements in the Central Apennines (central Italy). *Geomorphology*, 82, 201–
893 228. <https://doi.org/10.1016/j.geomorph.2006.05.003>

894 Galadini, F., Falcucci, E., Galli, P., Giaccio, B., Gori, S., Messina, P., Moro, M., Saroli, M.,
895 Scardia, G., Sposato, A., 2012. Time intervals to assess active and capable faults for
896 engineering practices in Italy. *Eng. Geol.* 139-140, 50-65.

897 Galli, P., Galadini, F., Pantosti, D., 2008. Twenty years of paleoseismology in Italy. *Earth-Science*
898 *Reviews*. 88, 89–117. <https://doi.org/10.1016/j.earscirev.2008.01.001>

899 Giraudi, C., Bodrato, G., Lucchi, M.R., Cipriani, N., Villa, I. M., Giaccio, B., Zuppi, G.M., 2011.
900 Middle and late Pleistocene glaciations in the Campo Felice Basin (central Apennines, Italy).
901 *Quaternary Research*, 75(1), 219-230. <https://doi.org/10.1016/j.yqres.2010.06.006>

902 Gomila, R., Arancibia, G., Mitchell, T.M., Cembrano, J.M., Faulkner, D.R., 2016.
903 Palaeopermeability structure within fault-damage zones: a snap-shot from microfracture
904 analyses in a strike-slip system *J. Struct. Geol.*, 83, 103-120, [10.1016/j.jsg.2015.12.002](https://doi.org/10.1016/j.jsg.2015.12.002)

905 Gratier, J.P., Dysthe, D., Renard, F., 2013. The role of pressure solution creep in the ductility of the
906 Earth's upper crust. *Advances in Geophysics*, 54, 47–179. [https://doi.org/10.1016/b978-0-12-](https://doi.org/10.1016/b978-0-12-380940-7.00002-0)
907 [380940-7.00002-0](https://doi.org/10.1016/b978-0-12-380940-7.00002-0).

908 Gundersen, E., Renard, F., Dysthe, D.K., Bjorlykke, K., Jamtveit, B., 2002. Coupling between
909 pressure solution creep and diffusive mass transport in porous rocks. *Journal of Geophysical*
910 *Research—Solid Earth*, 107. doi:10.1029/2001JB000287.

911 Hunstad, I., Selvaggi, G., D'Agostino, N., England Clarke, P., Pierozzi, M., 2003. Geodetic strains
912 in peninsular Italy between 1875 and 2001. *Geophys. Res. Lett.*, 30, 1828.

913 Hutchinson, J.N., 1988. General report: morphological and geotechnical parameters of landslides in
914 relation to geology and hydrogeology. *Proceedings of the 5th International Symposium on*
915 *Landslides*, Lausanne, CH, vol. 1. Balkema, Rotterdam, pp. 3±35.

916 Jaboyedoff, M., Penna, I., Pedrazzini, A., Baroň I., Crosta G.B., 2013. An introductory review on
917 gravitational-deformation induced structures, fabrics and modeling. *Tectonophysics*. 605, 1-
918 12. <https://doi.org/10.1016/j.tecto.2013.06.027>

919 Jahn, A., 1964. Slow morphological features resulting from gravitation. *Zeitschr. Geomorph.* 5, 59-
920 72.

921 Kim Y.S., Peacock D.C.P., Sanderson D.J., 2004. Fault damage zones. *Journal of Structural*
922 *Geology*, 26 (3), 503-517.

923 Kim, Y.S., Sanderson, D.J., 2005. The relationship between displacement and length of faults: a
924 review. *Earth-Science Reviews*. 68 (3-4), 317-334.

925 La Bruna, V., Agosta, F., Lamarche, J., Viseur, S., Prosser, G., 2018. Fault growth mechanisms and
926 scaling properties in foreland basin system: The case study of Monte Alpi, Southern
927 Apennines, Italy. *Journal of Structural Geology*, 116, 94-113.

928 Lavecchia, G., Brozzetti, F., Barchi, M., Menichetti, M., Keller, J.V.A., 1994. Seismotectonic
929 zoning in east-central Italy deduced from an analysis of the Neogene to present deformations

930 and related stress fields. *Geological Society of America Bulletin*, 106(9), 1107–1120.
931 [https://doi.org/10.1130/0016-7606\(1994\)106<1107:SZIECI>2.3.CO;2](https://doi.org/10.1130/0016-7606(1994)106<1107:SZIECI>2.3.CO;2)

932 Leah, H., Fondriest, M., Lucca, A., Storti, F., Balsamo, F., Di Toro, G., 2018. Coseismic extension
933 recorded within the damage zone of the Vado di Ferruccio Thrust Fault, Central Apennines,
934 Italy. *Journal of Structural Geology*, 114, 121–138. <https://doi.org/10.1016/j.jsg.2018.06.015>.

935 Lehner, F.K., 1995. A model for intergranular pressure solution in open systems. *Tectonophysics*,
936 245, 153–170.

937 Leonard, M., 2010. Earthquake fault scaling: Self-consistent relating of rupture length, width,
938 average displacement, and moment release. *Bulletin of the Seismological Society of America*,
939 100(5A), 1971-1988.

940 Lucca, A., Storti, F., Balsamo, F., Clemenzi, L., Fondriest, M., Burgess, R., Di Toro, G., 2019.
941 From submarine to subaerial out-of-sequence thrusting and gravity-driven extensional
942 faulting: Gran Sasso massif, central Apennines, Italy. *Tectonics*, 38, 4155–4184.
943 <https://doi.org/10.1029/2019tc005783>

944 Malinverno, A., Ryan, W.B.F., 1986. Extension in the Tyrrhenian Sea and shortening in the
945 Apennines as result of arc migration driven by sinking of the lithosphere. *Tectonics*, 5, 227–
946 245. <https://doi.org/10.1029/tc005i002p00227>.

947 Mancinelli, A., Chiocchini, M., Coccia, B., 2003. Orbitolinidae and Alveolinidae (Foraminiferida)
948 from the uppermost Albian-lower Cenomanian of Monti d'Ocre (Abruzzi, Italy). *Cretaceous*
949 *Res* 24, 729–741.

950 Mancinelli, P., Scisciani, V., Patruno, S., Minelli, G., 2021. Gravity modeling reveals a Messinian
951 foredeep depocenter beneath the intermontane Fucino basin (central Apennines).
952 *Tectonophysics*, 821, 229144, [10.1016/j.tecto.2021.229144](https://doi.org/10.1016/j.tecto.2021.229144)

953 Martino S., Prestininzi A., Scarascia Mugnozza G., 2004. Geological-evolutionary model of a
954 gravity-induced slope deformation in the carbonate central apennines (italy). *Quarterly journal*

955 of engineering geology and hydrogeology, 37(1): 31-47. <https://doi.org/10.1144/1470->
956 9236/03-030

957 Masoch, S., Fondriest, M., Preto, N., Secco, M., Di Toro, G., 2019. Seismic cycle recorded in
958 cockade-bearing faults (Col de Teghime, Alpine Corsica). *Journal of Structural*
959 *Geology*, 129, 103889. <https://doi.org/10.1016/j.jsg.2019.103889>

960 Masoch, S., Gomila, R., Fondriest, M., Jensen, E., Mitchell, T., Pennacchioni, G., Cembrano, J., Di
961 Toro, G., 2021. Structural Evolution of a Crustal-Scale Seismogenic Fault in a Magmatic Arc:
962 The Bolfin Fault Zone (Atacama Fault System). *Tectonics*,
963 40. <https://doi.org/10.1029/2021TC006818>

964 Masoch, S., Fondriest, M., Gomila, R., Jensen, E., Mitchell, T., Cembrano, J., Pennacchioni, G., Di
965 Toro, G., 2022. Along-strike architectural variability of an exhumed crustal-scale seismogenic
966 fault (Bolfin Fault Zone, Atacama Fault System, Chile). *Journal of Structural Geology*, 165,
967 104745.

968 Marshak, S., Haq, S.S.B., Sen., P., 2019. Ramp initiation in fold-thrust belts: Insight from PIV
969 analysis of sandbox models *J. Struct. Geol.*, 118, 308-323.

970 Mayolle, S., Soliva, R., Caniven, Y., Wibberley, C., Ballas, G., Milesi, G., Dominguez, S., 2019.
971 Scaling of fault damage zones in carbonate rocks. *J. Struct. Geol.*, 124, 35-50.

972 Mitchell, T.M., Faulkner, D.R., 2009. The nature and origin of off fault damage surrounding strike-
973 slip fault zones with a wide range of displacements: A field study from the Atacama fault
974 system, northern Chile, *J. Struct. Geol.*, 31, 802–816, doi:10.1016/j.jsg.2009.05.002.

975 Moro, M., Saroli, M., Tolomei, C., Salvi, S., 2009. Insights on the kinematics of deep-seated
976 gravitational slope deformations along the 1915 Avezzano earthquake fault (Central Italy),
977 from time-series DInSAR. *Geomorphology*, 112, 261–276. [https://doi.org/10.1016/j.](https://doi.org/10.1016/j.geomorph.2009.06.011)
978 [geomorph.2009.06.011](https://doi.org/10.1016/j.geomorph.2009.06.011)

979 Moro, M., Saroli, M., Gori, S., Falcucci, E., Galadini, F., Messina, P., 2012. The interaction
980 between active normal faulting and large scale gravitational mass movements revealed by

981 paleoseismological techniques: A case study from central Italy. *Geomorphology*, 151–152,
982 164–174. <https://doi.org/10.1016/j.geomorph.2012.01.026>

983 Ostermeijer, G., Mitchell, T., Aben, F., Dorsey, M., Rockwell, T., Fletcher, J., Ostermeijer, F.,
984 2020. Damage zone heterogeneity on seismogenic faults in crystalline rock; a field study of
985 the Borrego Fault, Baja California. *Journal of Structural*
986 *Geology*, 137, 104016. <https://doi.org/10.1016/j.jsg.2020.104016>

987 Panek, T., Klimeš, J., 2016. Temporal behavior of deep-seated gravitational slope deformations: A
988 review. *Earth-Science Reviews*, 156, 14-38.

989 Pantosti, D., D'Addezio, G., Cinti, F.R., 1996. Paleoseismicity of the Ovindoli– Pezza fault, Central
990 Apennines, Italy: a history including a large previously unrecorded earthquake in middle Ages
991 (890-1300). *J. Geophys. Res.* 101, 5937-5959.

992 Patacca, E., Scandone, P., 1989. Post-Tortonian mountain building in the Apennines. The role of
993 the passive sinking of a relic lithospheric slab. In: *The Lithosphere in Italy*, Eds. Boriani A.,
994 Bonafede M., Piccardo G.B. and Vai G.B. *Atti dei Convegni Lincei* 80, 157-176.

995 Patacca, E., Sartori, R., Scandone P., 1992a. Tyrrhenian basin and Apenninic arcs: kinematic
996 relations since late Tortonian times. *Mem. Soc. Geol. It.* 45, 425-451.

997 Peacock, D.C.P., Sanderson, D.J., 1991. Displacements, segment linkage and relay ramps in normal
998 fault zones, *J. Struct. Geol.* 13, 721-733.

999 Pollard, D., Aydin, A., 1988. Progress in understanding jointing over the past century. *Geological*
1000 *Society of America Bulletin*, 100, 1181–1204. [https://doi.org/10.1130/0016-](https://doi.org/10.1130/0016-7606(1988)100<1181:piujot>2.3.co;2)
1001 [7606\(1988\)100<1181:piujot>2.3.co;2](https://doi.org/10.1130/0016-7606(1988)100<1181:piujot>2.3.co;2)

1002 Power, W.L., Tullis, T.E., 1989. The relationship between slickenside surfaces in fine-grained
1003 quartz and the seismic cycle. *J. Struct. Geol.*, 11, 879-894.

1004 Renard, F., Gratier, J.P., Jamtveit, B., 2000. Kinetics of crack-sealing, intergranular pressure
1005 solution, and compaction around active faults. *Journal of Structural Geology*, 22(10), 1395–
1006 1407. [https://doi.org/10.1016/s0191-8141\(00\)00064-x](https://doi.org/10.1016/s0191-8141(00)00064-x)

- 1007 Renard, F., Dysthe, D., Feder, J., Bjørlykke, K., Jamtveit, B., 2001. Enhanced pressure solution
1008 creep rates induced by clay particles: Experimental evidence in salt aggregates. *Geophysical*
1009 *Research Letters*, 28, 1295–1298. <https://doi.org/10.1029/2000gl012394>
- 1010 Rovida, A., Locati, M., Camassi, R., Lolli, B., Gasperini, P., 2020. The Italian earthquake catalogue
1011 CPTI15. *Bulletin of Earthquake Engineering*, 18, 2953-2984. [https://doi.org/10.1007/s10518-](https://doi.org/10.1007/s10518-020-00818-y)
1012 [020-00818-y](https://doi.org/10.1007/s10518-020-00818-y)
- 1013 Rowe, C.D., Griffith, W.A., 2015. Do faults preserve a record of seismic slip: a second opinion. *J.*
1014 *Struct. Geol.* 78, 1-26.
- 1015 Rutter, E.H., 1983. Pressure solution in nature, theory and experiment. *Journal of the Geological*
1016 *Society*, 140, 725–740. <https://doi.org/10.1144/gsjgs.140.5.0725>.
- 1017 Salvi, S., Nardi, A., 1995. The Ovindoli Fault: a segment of a longer, active fault zone in central
1018 Abruzzi, Italy, in *Perspectives in Paleoseismology*, Vol. 6, pp. 101–113, eds Serva, L. &
1019 Slemmons, D.B., *Bull. Assoc. Eng. Geol.*
- 1020 Salvi, S., Cinti, F. R., Colini, L., D'addezio, G., Doumaz, F., Pettinelli, E., 2003. Investigation of the
1021 active Celano-L'Aquila fault system, Abruzzi (central Apennines, Italy) with combined
1022 ground-penetrating radar and paleoseismic trenching. *Geophysical Journal*
1023 *International*. 155(3), 805-818. <https://doi.org/10.1111/j.1365-246X.2003.02078.x>
- 1024 Savage, H.M., E.E. Brodsky., 2011. Collateral damage: Evolution with displacement of fracture
1025 distribution and secondary fault strands in fault damage zones, *J. Geophys. Res.*, 116,
1026 B03405, doi:10.1029/2010JB007665.
- 1027 Schirripa Spagnolo, G., Mercuri, M., Billi, A., Carminati, E., Galli, P., 2021. The segmented
1028 Campo Felice normal faults: seismic potential appraisal by application of empirical
1029 relationships between rupture length and earthquake magnitude in the central Apennines, Italy
1030 *Tectonics*, 40 (7).
- 1031 Sibson, R.H., 1977. Fault rocks and fault mechanisms. *Geological Society of London Journal*, 133,
1032 191–213. <https://doi.org/10.1144/gsjgs.133.3.0191>

- 1033 Sibson, R.H., 1986b. Earthquakes and rock deformation in crustal fault zones. *Ann. Rev. Earth*
1034 *Planet. Sci.* 14: 149–175.
- 1035 Sibson, R.H., 2003. Thickness of the seismic slip zone. *Bulletin of the Seismological Society of*
1036 *America*, 93, 1169–1178. <https://doi.org/10.1785/0120020061>
- 1037 Smith, S.A.F., Billi, A., Di Toro, G., Spiess, R., 2011. Principal slip zones in limestone:
1038 Microstructural characterization and implications for the seismic cycle (Tre Monti fault,
1039 Central Apennines, Italy). *Pure and Applied Geophysics*, 168(12), 2365–2393.
1040 <https://doi.org/10.1007/s00024-011-0267-5>.
- 1041 Smith, S.A.F., Nielsen, S., Di Toro, G., 2015. Strain localization and the onset of dynamic
1042 weakening in calcite fault gouge. *Earth Planet. Sci. Lett.*, 413, 25-36.
- 1043 Tada, R., Siever, R., 1989. Pressure solution during diagenesis. *Annual Review of Earth and*
1044 *Planetary Sciences*, 17, 89–118. <https://doi.org/10.1146/annurev.ea.17.050189.000513>.
- 1045 Tarquini, S., Isola, I., Favalli, M., Mazzarini, F., Bisson, M., Pareschi, M.T., Boschi, E., 2007.
1046 TINITALY/01: a new triangular irregular network of Italy. *Annals of Geophysics*, 50, 407-
1047 425.
- 1048 Tesei, T., Collettini, C., Viti, C., Barchi, M.R., 2013. Fault architecture and deformation
1049 mechanisms in exhumed analogues of seismogenic carbonate-bearing thrusts *J. Struct.*
1050 *Geol.*, 55, 167-181.
- 1051 Varnes, D.J., 1978. Slope movements types and processes. In R. L. Schuster, & R. J. Krizek (Eds.),
1052 *Landslides: Analysis and control*, pp. 11-35.
- 1053 Vezzani, L., Festa, A., Ghisetti, F.C., 2010. Geology and tectonic evolution of the Central-Southern
1054 Apennines, Italy. *Geological Society of America Special Paper*, 469, 1–58.
1055 <https://doi.org/10.1130/2010.2469>
- 1056 Villani, F., Pucci, S., Civico, R., De Martini, P.M., Cinti, F.R., Pantosti, D., 2018. Surface faulting
1057 of the 30 October 2016 Mw 6.5 Central Italy earthquake: Detailed analysis of a complex
1058 coseismic rupture. *Tectonics*. 37, 3378–3410. <https://doi.org/10.1029/2018TC005175>

- 1059 Wells, D.L., Coppersmith, K.J., 1994. New empirical relationships among magnitude, rupture
1060 length, rupture width, rupture area, and surface displacement. *Bulletin of the seismological*
1061 *Society of America*, 84(4), 974-1002.
- 1062 Wesnousky, S.G., 2008. Displacement and geometrical characteristics of earthquake surface
1063 ruptures: Issues and implications for seismic-hazard analysis and the process of earthquake
1064 rupture. *Bulletin of the Seismological Society of America*, 98(4), 1609-1632.
- 1065 Wibberley, C.A.J., Yielding, G., Di Toro, G., 2008. Recent advances in the understanding of fault
1066 zone internal structure: a review. *Geol. Soc. Lond. Spec. Publ.* 299, 5–33.
1067 <https://doi.org/10.1144/SP299.2>.
- 1068 Wilkinson, M., Roberts, G.P., McCaffrey, K., Cowie, P. A., Walker, J.P.F., Papanikolaou, I.,
1069 Richard, J.P., Michetti, A.M., Vittori, E., Gregory, L., Wedmore, L., Watson, Z.K., 2015. Slip
1070 distributions on active normal faults measured from LiDAR and field mapping of geomorphic
1071 offsets: an example from L'Aquila, Italy, and implications for modelling seismic moment
1072 release. *Geomorphology*, 237, 130-141.
- 1073 Woodcock, N.H., and K. Mort., 2008. Classification of fault breccias and related fault
1074 rocks. *Geological Magazine* 145, no. 3: 435– 440.
- 1075 Zischinsky, U., 1966. On the deformation of high slopes (Vol. 2, pp. 179–185). 1st Conference on
1076 International Society for Rock Mechanics.
- 1077 Zischinsky, U., 1969. Uber Sackungen. *Rock Mechanics*, 1, 30–52.
1078 <https://doi.org/10.1007/bf01247356>